University of Nottingham
UK | CHINA | MALAYSIA

Masters of Research in Neuroscience
2021-2022

Thesis Title:

The Differential Sensitivity of Adult Mouse Optic Nerve Axon Sub-populations to High Frequency Firing

Author:

Hana Beswick-Jones

Word Count: 19,480

Acknowledgments

I would like to express my gratitude to my supervisor Dr. Angus Brown for his invaluable and constant guidance throughout this Research project, making this be a truly enjoyable and insightful year. I would also like to express my thanks for the opportunity to write and publish papers under his guidance, with two papers already published and many others under review for publication. This has been a year which I will remember fondly as I progress into my new career in physiology.

I would also like to thank my lab partner Amy Hopper, who has been there throughout to experience both the fun and challenging times this year. Her support and knowledge have been essential to my progress and I couldn't have asked for a better lab partner.

Finally, I would like to thank my family and Dan for always supporting and encouraging me throughout my academic studies. Their enthusiasm and attempts to understand as I proudly explain seemingly meaningless figures will always be appreciated.

Table of Contents

Abstract ***5***

Chapter 1: Introduction ***6***

1.1 The origins of membrane potential **6**

1.1.2 The action potential 7

1.1.3 Energy requirements and conduction 11

1.2 The distribution of axon calibre **12**

..... 14

1.2.1 Axon sub-populations 15

1.3 Models of metabolic challenge **18**

1.3.1 The K^+ theory of CAP failure 19

1.3.2 K^+ clearance from the extracellular space 20

1.3.3 The Na^+ theory of CAP failure 23

Chapter 2: Methodology ***25***

2.1 Ethics approval **25**

2.2 Dissection 25

2.3 Electrophysiology **26**

..... 28

2.4 K^+ sensitive microelectrodes 29

2.5 K^+ Calibration 32

2.6 Curve fitting and data analysis **33**

2.7 Calculation of $[Na^+]_i$ 34

Chapter 3: Results ***35***

3.1 The effects of increasing stimulus voltage on CAP recruitment **35**

3.2 The effects of reducing the time interval between frequency stimulations. **40**

..... **43**

..... **43**

3.3 The response of the three CAP peaks to varying stimulus frequency. **44**

3.3.1 The effects of low frequency stimulation on CAP amplitude. 45

3.3.1The effects of high frequency stimulation on CAP amplitude 46

3.4 The effects of decreasing $[Na^+]_o$ on CAP amplitude **48**

3.5 The effects of increased $[K^+]_o$ on CAP amplitude **55**

3.6 A summary of the effects of high frequency stimulation on $[K^+]_o$, CAP amplitude, CAP profile and $[Na^+]_i$. **72**

Chapter 4: Discussion ***73***

4.1 Evidence for the existence of three distinct sub-populations of axon diameter. **74**

4.1.2 Larger diameter axons within the MON facilitate higher information transfer rates and neuronal firing. 76

4.2 Evidence disputing $[K^+]_o$ as the driving force for CAP fall during high frequency firing. **77**

4.3 $[Na^+]_i$ accumulation during high frequency firing. **80**

4.3.1 The differential sensitivity of axon sub-populations to accumulating $[Na^+]_i$ 81

4.4 The role of $[K^+]_o$ in CAP recovery **83**
Conclusion ***84***
References ***86***

Abstract

Extracellular recordings of the stimulus evoked compound action potential (CAP) from the mouse optic nerve (MON) display a triphasic profile indicative of the presence of three axon sub-populations of discrete conduction velocity (CV) based on axon size. While larger diameter axons are known to increase CV, the MON is a short central nervous system (CNS) tract and an increase in axon diameter would only marginally increase information arrival time. Therefore, we propose that larger diameter axons exist in the MON to facilitate higher information transfer rates and neuronal firing frequency. The largest axons were most resistant to high frequency stimulus, maintaining their profile while those of the second and third peaks fell in amplitude and increased in latency.

The original dogma suggests that this fall in CAP amplitude is due to accumulating extracellular K^+ ($[K^+]_o$) which is liberated from the axons during the repolarising phase of the action potential. The use of K^+-sensitive microelectrodes demonstrated that the CAP amplitude does not begin to fall until $[K^+]_o$ is >9 mM. However during a 100 Hz stimulation for 2 minutes, $[K^+]_o$ only accumulated to ~4 mM due to powerful astrocytic buffering. Therefore, we propose that the CAP amplitude does not fall during high frequency firing due to $[K^+]_o$, but alternatively accumulating intracellular Na^+ ($[Na^+]_i$) which enters axons during stimulation. It proves impossible to achieve accurate real-time measurements of $[Na^+]_i$ in small central axons. Therefore, indirect methods were used through manipulation of the Nernst equation. The first peak was predicted to accumulate the least $[Na^+]_i$, reaching 22.3 mM (SD = 13.0) at 100 Hz stimulation, followed by the second peak 44.7 mM (SD = 10.3) and the third peak, which accumulated $[Na^+]_i$ to the greatest extent, reaching 62.9 mM (SD = 9.5) during stimulation. We propose that the differential manner with which the three CAP peaks accumulate $[Na^+]_i$ is due to the surface area-to-volume considerations of varying sized axons, as larger diameter axons possess a higher mitochondrial fraction volume as compared to membranous Na^+/K^+/ATPase pumps. Therefore, they have a greater capacity to extrude $[Na^+]_i$ following high frequency firing.

Chapter 1: Introduction

1.1 The origins of membrane potential

The basic mammalian cell resides in chemical disequilibrium, with the intracellular ionic composition decidedly different from that of the extracellular. The predominant intracellular cation is K^+ which is present at a concentration 10-fold higher than that found within the extracellular milieu (Zacchia et al., 2016). Conversely, the dominant cation found extracellularly is Na^+. This disequilibrium is maintained by the cell membrane and its energy dependent transportation systems (Pirahanchi and Aeddula, 2019). However, the first protocells to emerge could not possess ion-tight membranes, or the pumps required for the maintenance of transmembrane ion gradients. It is therefore proposed that the ionic composition of the modern cell is a consequence of the environment in which protocells first originated over 3.5Gy ago. Contrary to the common belief that life originated in marine environments, geothermal analysis suggests that this 'hatchery' may have been terrestrial geothermal fields (Mulkidjanian et al., 2012). In the anoxic primordial atmosphere, these fields comprised Na^+ and K^+ concentrations resembling that of the modern intracellular milieu, in addition to the presence of essential small inorganic compounds (Mulkidjanian et al., 2012). Therefore, all of the necessary constituents to form the first replicating self-contained organisms on earth were present in this environment.

It is hypothesised that the subsequent dispersion of organisms along rivers would lead to their emergence in oceans containing high [Na^+]- an environment unequivocally different in ionic composition than that of geothermal fields and consequently, found within cells. Without the implementation of a system to maintain the established milieu of cells, Na^+ would rapidly influx down its concentration gradient and accumulate intracellularly, creating osmotic complications (Armstrong, 2005). The evolution of the first Na^+/K^+ ATPase pumps were therefore essential to actively remove Na^+ from the cell in exchange for K^+. The stoichiometry of this electrogenic transporter is considered to be 3:2,

precipitating the cotransport of three Na^+ out of the cell for every two K^+ transported into the cell, per catalytic cycle (Pirahanchi and Aeddula, 2019). Due to the energy demand to expedite this transport, glycolysis became the obligate source of adenosine 5'-triphosphate (ATP) to fuel the pumps. Cells consequently reside in chemical disequilibrium and a transmembrane potential difference across the membrane is generated, as present in the modern cell. This proposition of cell evolution is in accordance with the "chemistry conservation principle" proposed by McCallum, which suggests that cellular chemistry is more conserved than that of the evolving environment surrounding them. The basic eukaryotic cell is therefore proposed to have evolved from the same model, now found ubiquitously in every animal (excluding a small number of exceptions such as the red blood cell which is predominantly permeable to Cl^-, as opposed to K^+ (Passow, 1964)). The composition of our blood supports this theory of evolution, existing as essentially diluted seawater, reflecting the environment in which these organisms first emerged. The formation of life on earth took 2/3 of the duration of the Universe's existence, however it was only in the most recent billion years that the evolution of multicellular organisms took place (Niklas and Newman, 2013), reflecting the complexity of maintaining a multicellular system.

1.1.2 The action potential

The significance of the electrical potential difference across a plasma membrane is difficult to exaggerate in terms of physiology. Vertebrates first took advantage of the steep Na^+ gradient across the cell membrane to permit the rapid influx of Na^+ through voltage-gated ion channels. The emergence of multicellular organisms could then utilise this mechanism to facilitate long distance communication between cells, generating the electrical impulses which underpin the nervous system. It was the historical work of Hodgkin and Huxley commencing in 1939, which provided the first fundamental insight into the mechanisms underpinning this nerve cell excitability and axonal conduction (Hodgkin and Huxley, 1939). Through the insertion of a microelectrode down the length of a squid giant axon, the first intracellular action potential could be

recorded between the nerve fibre and the conducting extracellular solution surrounding it. It would be technically difficult, if not impossible to record directly from most axons due to their size, however the remarkably large lumen characterised by the squid giant axon could be exploited to permit such electrophysiological recordings. Hodgkin and Huxley proceeded to deduce the co-ordinated changes in membrane permeability, coupled with transmembrane ion fluxes that produce the propagating action potential and through ingenious manipulation of mathematical equations, were able to model the action potential. One example of this is the adaption of the Nernst equation, used to predict the potential difference created by the uneven distribution of ions between the cell compartments and the extracellular fluid (Hopper et al., 2022). The application of this physico-chemical law to membrane biophysics allowed further understanding of the excitable axon membrane and its varying permeability during the different phases of the action potential. It is established that when an ion's reversal potential (Ex) does not equal the membrane voltage (Vm), the ion will cross the membrane in the direction that drives Vm towards Ex. With this understanding, it was shown by Hodgkin and Katz that the resting membrane potential in squid giant axon was -45mV, and +40mV at the peak of the action potential following stimulation; close to the estimated reversal potential of Na^+ (ENa) (Hodgkin and Katz, 1949). This was highly suggestive that during the depolarising phase of the action potential the membrane becomes transiently permeable to Na^+, permitting rapid Na^+ influx to drive the Vm towards ENa. This hypothesis was experimentally confirmed by a quantitative reduction in action potential amplitude when the [Na^+] in seawater bathing the nerves was decreased, as seen in figure 1A. This decrease in amplitude was as predicted when the difference between the ENa in normal seawater and E'Na in reduced [Na^+] seawater was calculated (Hodgkin and Katz, 1949). This concept of transient Na^+ membrane permeability was later confirmed by Hodgkin and Huxley who exploited a double-step protocol in concert with the voltage clamp technique to enable the recording of membrane currents evoked in response to fixed voltages (Hodgkin and Huxley, 1952a). However, importantly, the implementation of this technique additionally permitted investigations into K^+

membrane permeability. A wide range of membrane voltages were tested, from ~-65mV, to beyond ENa, producing an early transient inward current, followed by a sustained outwards current. It was suggested that this outward current was as a result of delayed K^+ efflux from the axon during the repolarising and after hyperpolarisation (AHP) phases of the action potential. This was therefore investigated by replacing the Na^+ in artificial seawater with the impermeant ion choline (minus a small residual percentage of Na^+ which must remain in the solution to counteract the increased resistance imposed by choline). It was then possible to isolate the Na^+ current by subtracting the choline traces from the seawater traces, from which the outwards current thought to be K^+ could in turn, be estimated by subtracting the Na^+ current from the seawater currents (Hodgkin and Huxley, 1952a). Further experiments were carried out by Keynes who used radioactive tracers to quantify membrane ion changes (Keynes, 1951). The use of radioisotopes offered the advantage that influx and efflux could be measured independently, as opposed to the measure of currents, which provides limited information being the summation of ion fluxes. It is therefore indisputable that the ingenious work of Hodgkin and Huxley, as well as others, vastly increased our understanding of cell excitability and laid the foundation for the investigations into membrane biophysics that we conduct today.

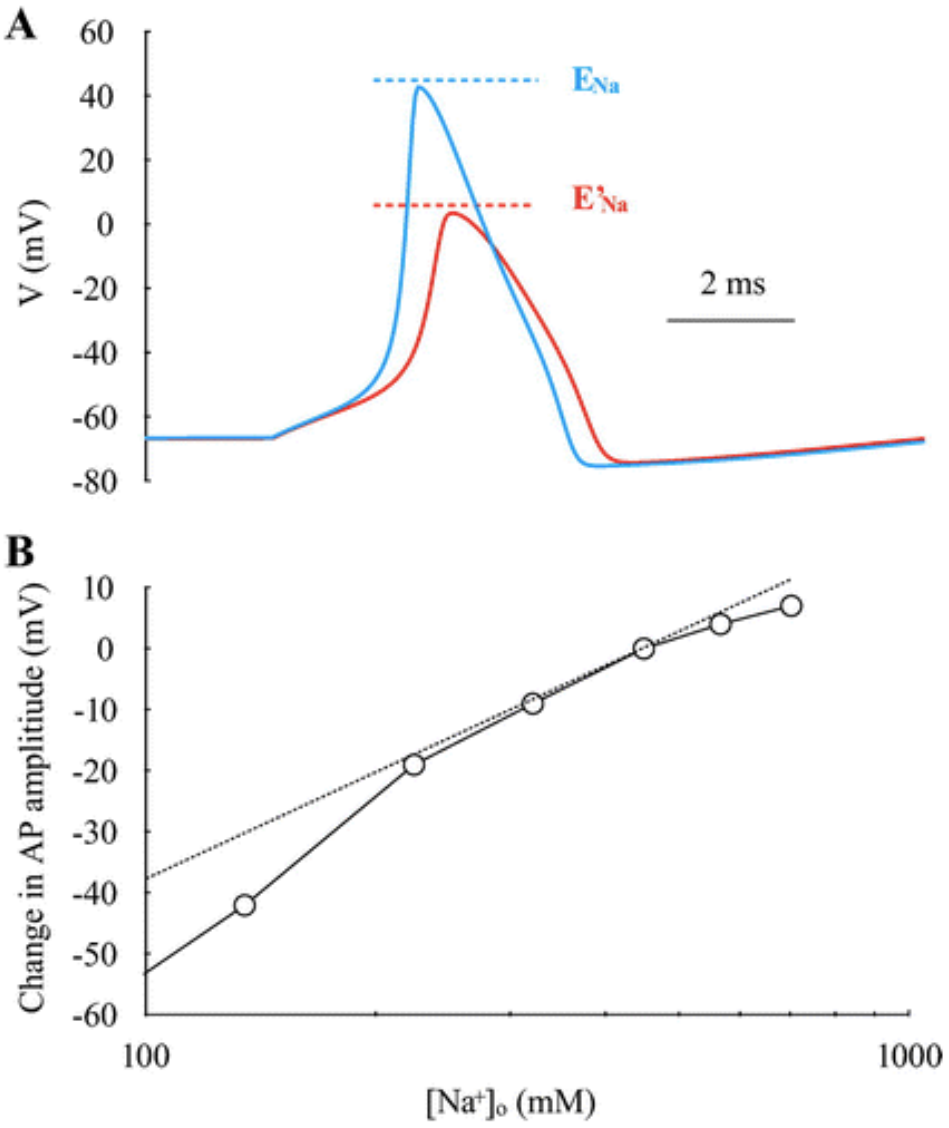

Figure 1.

A simulation of the experiments carried out by Hodgkin and Katz (1949), quantifying the effects of reducing [Na^+] in seawater on action potential amplitude. A: The peak of the action potential in normal seawater (blue trace) approaches ENa at ~45mV. When the [Na^+] is reduced (red trace), the action potential amplitude decreases towards the new E'Na of ~5mV. B: The change in action potential amplitude was predicted (dotted line) by calculating the difference between ENa in the normal and reduced [Na^+] seawater. The actual amplitudes recorded (open circles) can be seen to closely follow those predicted *(Hopper, Beswick-Jones and Brown, 2022).*

1.1.3 Energy requirements and conduction

Due to the importance of the electrical potential difference across a cell membrane, it is imperative that mechanisms exist to maintain the transmembrane ion gradients. Without the continual activity of the Na^+/K^+ ATPase to redistribute ions, gradients would dissipate over time inhibiting the organism's ability to evoke a new action potential and maintain cell-to-cell communication. However, constant maintenance of these gradients requires considerable energy which has increased as a non-linear function with animal size and complexity. This can be demonstrated in humans, where the brain constitutes 2% of body weight, however, receives ~20% of resting cardiac output (Veenith and Menon, 2011). This blood flow devoted to the brain ensures that sufficient glucose and oxygen is delivered to active regions for oxidative phosphorylation and subsequent ATP synthesis.

In conjunction with the elevated demand of energy with animal size, the necessity for long-distance communication also increased (More and Donelan, 2018). It is an evolutionary advantage for primitive animals to be capable of fast conduction in longer central nervous system (CNS) tracts, especially those responsible for escape reflexes. The nervous systems have evolved two basic mechanisms to increase the speed of axonal conduction and action potential propagation, the first of which is axon gigantism. By favouring greater axon diameter, the axonal length constant increases exponentially due to axoplasmic conductance, therefore increasing the conduction velocity of the electrical impulse (Hartline and Colman, 2007). The most extensively researched example of this is observed in the *Loligo* squid, which possesses a giant axon responsible for rapid mantle contraction upon stimulation. This results in jet-propelled expulsion of seawater from the siphon and vigorous escape from predation (Otis and Gilly, 1990). A further example can be observed in the sciatic nerve- the longest and largest nerve in the human body, providing an evolutionary advantage for rapid motor function and successful predatory-prey interactions, in accordance with the conduction-time hypothesis. The second mechanism for

increasing conduction speed in the nervous system is to ensheathe axons in helical or concentrically wrapped sheets of myelin (Waxman and Bennett, 1972). The convergent evolution and conservation of myelin across multiple taxa, (i.e., it did not evolve from a common ancestor) demonstrates the importance in promoting survival through parallel computation (Hartline and Colman, 2007). The tight lipid-rich multilamellar wraps reduce the axonal membrane capacitance, favouring current travel along the axon. Additionally, the termination of myelin at the axonal nodes reduces the area of membrane through which current can flow, facilitating saltatory conduction (Rosenbluth, 2009). This therefore increases the velocity at which the electrical impulse arrives at the nerve terminal. Myelinated axons consequently have a linear relationship between conduction velocity and axon diameter, compared to a squared relationship in unmyelinated axons. Therefore, larger axon diameter was thought to facilitate faster axon conduction. However, this hypothesis must be questioned when applied to short CNS tracts such as the optic nerve, observed to possess a wide range of myelinated axon diameters.

1.2 The distribution of axon calibre

The diameter of myelinated axons within the nervous system is largely varied, differing by nearly 100-fold (~0.2-20μm) (Susuki, 2010). Due to the space and energy constraints imposed by larger axons, it would be expected that thicker fibres predominate in longer neural tracts where faster conduction is required. Thinner fibres could then be restricted to shorter CNS tracts where information arrival time would be reduced by only a fraction; however, this is not the case (Friede et al., 1984). A prominent example of this is seen in the optic nerve which despite being a relatively short CNS tract, comprises a highly skewed distribution of axon calibre (Perge et al., 2009). Perge and colleagues found that in guinea pig, the optic nerve conduction distance to the lateral geniculate nucleus (LGN) is short (17 mm), and the difference in conduction times between the thickest and thinnest axon diameters is only ~3.2 ms. This is considerably shorter than the

typical temporal response variability of 10-30 ms in response to a repetitive stimulus (Perge et al., 2009). Therefore, larger axonal diameters in the optic nerve are unlikely to enhance the detection of a visual stimulus. As a result, it seems implausible that the brain would devote such substantial proportions of space and energy for a negligible increase in information arrival time. Due to evolutionary redundancy, a further explanation must exist. It is therefore proposed in shorter CNS tracts, that although larger diameter axons do conduct faster, they exist to facilitate higher information transfer rates and neuronal firing frequency. It has been shown within the optic nerve that the mitochondrial density rises linearly with axon diameter ≤0.7µm, whereas this relationship becomes quadratic when diameter is >0.7µm (Perge et al., 2009). Therefore, for a two-fold increase in axon diameters >0.7µm, the volume increase will be quadratic as compared to surface area, as illustrated in figure 2. Consequently, there is a greater mitochondrial volume fraction present in proportion to membranous ion channels localised to the surface. This permits an elevation in the quantity of ATP produced and thus, a greater capacity to deal with the metabolic demands generated by high frequency firing, such as the re-equilibration of transmembrane ion gradients. Larger axons are therefore intrinsically advantageous to propagate high-frequency spiking, as compared to those with a smaller diameter. There is no doubt that in longer CNS tracts the conduction time hypothesis stands, however this alternative proposition provides a holistic explanation for the distribution of axon calibre within shorter tracts.

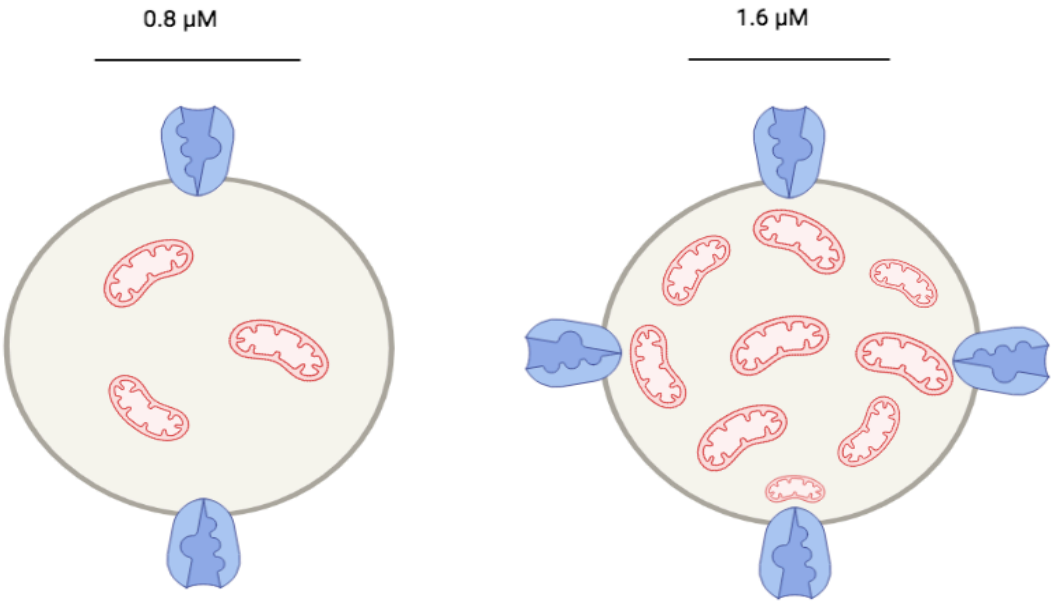

Figure 2.

As an axon doubles in diameter from 0.8µm to 1.6µm, surface area increases linearly, while axon volume increases as a squared function. Membranous ion channels localised to the surface therefore undergo a 2-fold increase compared to the mitochondria localised to the axon volume which experience a quadratic increase.

1.2.1 Axon sub-populations

The optic nerve, cranial nerve II, proves a useful model of central white matter not only due to its accessibility, but also because of its lack of complications imposed by cell bodies or glutamatergic synapses due to its exclusive composition of myelinated axons and glia (Evans et al., 2010). This is enhanced by its ability to withstand long periods of *ex-vivo* metabolic investigation (Allen et al., 2006). Electrophysiological recordings of the optic nerve when imposed with a supramaximal stimulus generates a characteristic triphasic compound action potential (CAP) profile, as seen in figure 3, representing the summed currents from all conducting axons within the tract (Stys et al., 1991). Morphological studies using electron microscopy techniques suggest that the MON consists of ~25,000 myelinated axons varying in diameter from 0.2 to 2.7 µm (Allen et al., 2006). Due to the nature of action potential firing to be all or nothing, a fall in stimulus-evoked CAP area can therefore be assumed to indicate a decrease in the number of axons contributing to the CAP as a result of metabolic disruption (Evans et al., 2010). The CAP proves a reliable index of nerve function; however, is complex to analyse due to being accurately fit by multiple Gaussian functions, as seen in figure 3. Fortunately, curve fitting procedures can be utilised for quantitative resolution into constituent peaks (Evans et al., 2010).

Allen et al. (2006) proposed that this triphasic profile is generated by three distinct sub-populations of axon diameters, with the largest axons contributing to the first peak, intermediate sized to the second peak and smallest to the third. This is demonstrated by the first peak being recruited at the lowest stimulus intensity, followed by the second and third peaks, respectively. This therefore suggests that the axons contributing to the first peak comprise those with the lowest threshold for activation, known to be thicker fibres with lower axoplasmic resistance. This is further supported by the first peak displaying the shortest latency to peak when stimulated, followed by the second peak and finally the third. This suggests that the first peak is contributed to by axons with the fastest conduction velocities, characterised by a larger diameter. It is therefore proposed that during the application of increasing frequency stimulus to the

mouse optic nerve (MON), the third peak would be lost first due to the smaller axons having a lower capacity to withstand the high metabolic demands. This would then be followed by failure of the second peak comprising the intermediately sized axons and finally, the first peak which retains the highest capacity to accommodate the re-equilibration of transmembrane ion gradients. This is a hypothesis which we aim to experimentally investigate.

The MON CAP has also demonstrated metabolic diversity among its three peaks. It has been shown by Meakin et al (2007), that when 10mmol/L glucose is substituted for 10mmol/L fructose in the aCSF bathing the nerves, there is a delayed loss in the first peak, while the second and third peaks remain unaffected. However, when tissue glycogen stores were depleted via prior exposure to aglycaemia or high frequency firing, fructose was determined to be incapable of sustaining the first peak of the CAP. This was proposed to be as a result of a discrepancy in the expression of fructokinase between the axons, responsible for the phosphorylation and efficient metabolization of fructose. Enzyme assays showed that fructokinase was expressed in the axons contributing to both the second and third peaks of the CAP, however not in the fast-conducting larger diameter axons comprising the first peak (Meakin et al., 2007).

Similar metabolic diversity has also been demonstrated in the peripheral nervous system (PNS). It has been proposed that both A and C fibres within the sciatic nerve can utilise fructose in order to sustain function. However, where C fibres are likely to utilise fructose directly, in the larger diameter A fibres fructose must first be metabolised to lactate in local Schwann cells for utilisation (Rich and Brown, 2018). This therefore demonstrates unique metabolic profiles of the axons contributing to the CAP and axons can therefore not be considered a homogenous population with regards to their metabolic characteristics (Evans et al., 2010).

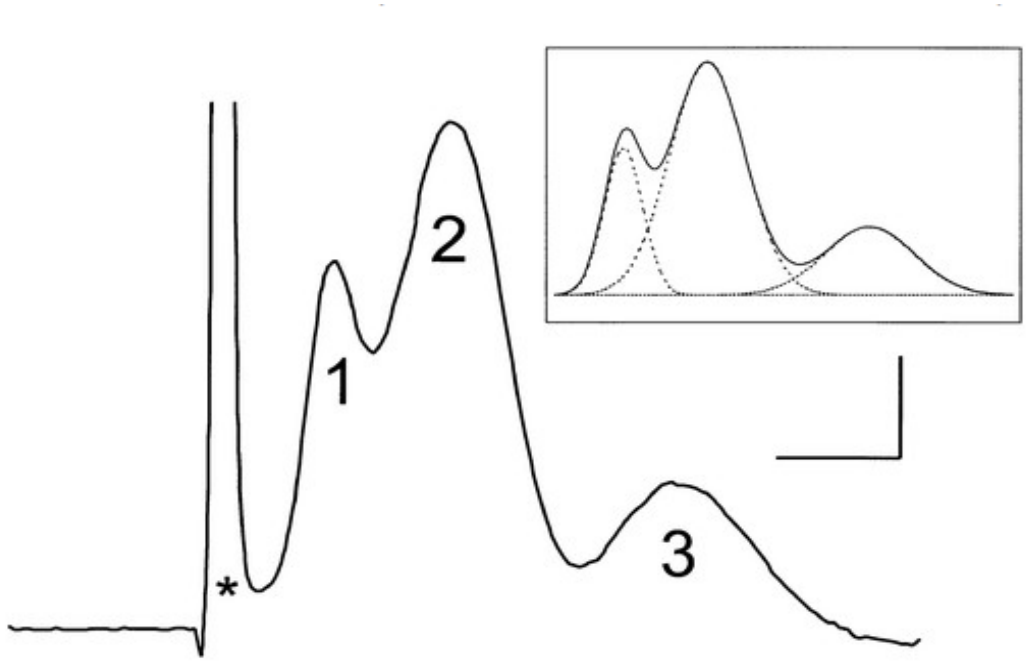

Figure 3.

A schematic of a compound action potential (CAP) which is obtained from electrophysiological recordings of the optic nerve, during a supramaximal stimulus. The CAP occurs immediately after the stimulus artifact (*) and displays a characteristic three-peak profile (1,2 and 3), likely to be contributed to by three distinct sub-populations of axon diameter. Scale bars are 1mV and 1ms. *Insert:* represents the best fit Gaussian function for each of the 3 peaks. *(Allen et al., 2006)*

1.3 Models of metabolic challenge

There exist several ways to impose metabolic challenge upon a nerve in order to investigate the subsequent effects on CAP profile. Metabolic 'challenges' impose energy demands on the tissue which exceed its normal baseline levels, which can include physiologically relevant challenges such as imposing high frequency firing, or pathological challenges such as anoxia (Tekkök et al., 2003), aglycaemia (Brown et al., 2003) or the two combined – ischemia (Tekkök et al., 2007). Additionally, exposure to metabolic toxins such as cyanide and iodoacetate can be exploited for experimental purposes (Beck et al., 1982) (Stys, 2004). These metabolic challenges limit the production of ATP resulting in a discrepancy between energy supply and its demand. This consequently results in failure of the Na^+/K^+/ATPase and accumulation of intracellular Na^+ (Stys, 2004), instigating functional failure of the tissue as indicated by a fall in CAP area. However, the energy constraints imposed by physiological challenges such as high frequency firing can be met via functional hyperaemia, where an increase in blood flow to the active area can deliver an increased supply of energy substrate and oxygen. This therefore permits the nerve to accommodate for such metabolic challenges under physiological circumstances. It is not beyond reason to assume that the nerve conducts at high frequencies for very limited periods of time. However, at exceptionally high stimulus frequencies, the system becomes overwhelmed and functional hyperaemia is no longer sufficient to sustain neuronal firing.
The CAP proves a reliable measure of metabolic injury in central white matter injury, as the area of the peaks pre- and post-insult indicates the degree of damage incurred by the nerve. This has therefore been utilised as an index of axon injury under acute metabolic challenges such as anoxia, hypoxia, aglycaemia and ischaemia (Bastian et al., 2020). The MON has become a favoured model to investigate such metabolic challenges and has recently replaced the frequently used rat optic nerve for research. This transition permits exploitation of the shorter diffusion distance observed in the MON, which proves advantageous during *in vitro* metabolic studies where nutrients is circumvented

(Allen et al., 2006). Furthermore, the use of mouse models ensures compatibility with future transgenic and spontaneous mutant models.

1.3.1 The K^+ theory of CAP failure

The mechanisms underpinning the progressive failure of the CAP during high frequency stimulation are in need of further investigation. During neuronal activity, K^+ is extruded from the axon into the extracellular space as the action potential repolarises (Hodgkin and Huxley, 1953), where it accumulates to an appreciable extent (Frankenhauser and Hodgkin, 1956). With each individual action potential, the same [K^+] is liberated from the axon (Hodgkin and Huxley, 1947). Therefore, its accumulation in the extracellular fluid is linear and proportional to stimulus frequency (Frankenhauser and Hodgkin, 1956) (Baylor and Nicholls 1969). It was estimated that with each individual action potential, the $[K^+]_o$ rises by ~0.8-1mM (Frankenhauser and Hodgkin, 1956), however repetitive or high frequency stimulation can cause a greater elevation. This large quantity of positively charged K^+ within close proximity to the axonal membrane would act to depolarise it, preventing the recovery of Na^+ channel inactivation (Hodgkin and Huxley, 1952b). This inactivation consequently reduces the number of channels available for Na^+ to move through and therefore decreases the rate of membrane depolarisation, in addition to CAP peak amplitude which is determined by ENa. With this understanding, it was proposed that activity dependent K^+ accumulation may be the cause of CAP failure with high frequency firing. Under these circumstances, this hypothesis appears as a highly plausible explanation for CAP failure, however, there remain a few factors which have not been taken into consideration.

The foundation for this hypothesis relies on the seminal work of Frankenhauser and Hodgkin (1956), who conducted their investigations in the *Loligo* squid. Although the squid giant axon has proved as an indispensable model for investigating *in-vivo* cell excitability, it retains some fundamental physiological differences which make its generalisability dubious, the most pivotal of which is the existence of an unselective external barrier. This barrier has been shown to

be localised approximately 300 Å from the squid giant axon membrane and acts to confine K^+ within close proximity to the excitable cell membrane, preventing it from freely diffusing away (Frankenhauser and Hodgkin, 1956). Consequently, K^+ accumulates in the aqueous solution between the membrane and the external barrier. However, most axons aside from the squid giant axon, including the myelinated optic nerve, do not possess this 'external barrier' which confines K^+ to the axolemma. Furthermore, this theory does not acknowledge the propensity of astrocytes to spatially buffer extracellular K^+.

1.3.2 K^+ clearance from the extracellular space

It is appreciated that astrocytes are exclusively permeable to K^+, which causes the astrocytic membrane potential to be very sensitive to changes in $[K^+]_o$, varying logarithmically as predicted by the Nernst equation (Orkand et al., 1966). As a result, the reversal potential of K^+ (E_K) determines the astrocytic membrane voltage (Vm), i.e E_K = Vm. Glial spatial buffering relies on the membrane potential of astrocytes localised to areas of high neuronal activity being negative relative to the reversal potential of K^+, as seen in figure 4. This therefore provides a driving force for the uptake of K^+ into the intracellular space of astrocytes in an attempt to achieve equilibrium between Vm and E_K (Kofuji and Newman, 2004). Sequential action potentials result in depolarisation of the glial cell membrane of diminishing amplitude, as predicted by the Nernstian relationship between $[K^+]_o$ and membrane potential (Orkand et al., 1966). K^+ can in turn be spatially buffered along its concentration gradient, throughout the astrocytic syncytium via gap junctions. An Na^+/K^+/ATPase isoform is expressed on the glial cell membrane and has been implicated in the active uptake of K^+ and its redistribution from the extracellular space. These pumps are sensitive to $[K^+]_o$ around the physiological concentration of ~3mM and respond instantaneously by adjusting their rate of K^+ uptake. Studies have supported this, demonstrating that the inhibition of Na^+ pumps with 50μM strophanthidin before a 100Hz

stimulus for 1 second attenuates the post-stimulus recovery of $[K^+]_o$ (Ransom et al., 2000).

Although most evidence suggests that the Na^+/K^+/ATPase is the predominant K^+ clearance mechanism, glial inwards rectifying K^+ channels (Kir) have also been proposed to be involved (Bay & Butt, 2012). It was shown in the adult MON by Bay and Butt (2012), that as frequency stimulation increased from 1 Hz to 10-35 Hz for 120 seconds, $[K^+]_o$ rapidly increased in a frequency dependent manner, accompanied by a fall in the CAP amplitude. However, the specific blockade of the Kir subtype Kir1.4 with 100μM $BaCl_2$ resulted in a slowed post-stimulus recovery of $[K^+]_o$ and CAP at all stimulus frequencies. In addition to this, at higher levels of axonal activity, Kir blockade increased extracellular K^+ accumulation, therefore exacerbating CAP failure. This suggests that Kir1.4 channels do contribute to the clearance and spatial buffering of extracellular K^+ during neuronal activity.

It was shown by Frankenhauser and Hodgkin (1956), that as axons fired at a high frequency, $[K^+]_o$ began to accumulate outside of the axolemma, causing the action potential to fall in amplitude. However, without the external barrier observed in the *Loligo* squid to confine K^+, it is free to diffuse towards local glial cells for sequestration, maintaining a physiological ceiling level of extracellular K^+. This level is therefore highly unlikely to reach a physiological concentration capable of imposing the onset of CAP failure. Therefore, it does not appear that the reason for CAP failure is as a result of extracellular K^+ preventing Na^+ channel inactivation.

This effect is observed to be dependent on maturation, due to changes in activity dependent K^+ accumulation with postnatal age and tissue maturity (Connors et al., 1982). It has been demonstrated that in the optic nerve of 1-3 day old rats, the maximal $[K^+]_o$ evoked by optimal frequencies of stimulation was 17.2 mM, compared to 9.8 mM in adult optic nerve (Connors et al., 1982). This significant difference in the ceiling level $[K^+]_o$ is thought to be as a result of astrocytic immaturity in younger rodents. This has been demonstrated by administration of the mitotic inhibitor 5-azacytidine (5-AZ) to neonatal rat optic nerve, which is known to disrupt gliogenesis. Upon administration, animals older than 5 days

showed a significantly higher activity dependent accumulation of $[K^+]_o$, as compared to control animals, in addition to a larger CAP profile (Yamate and Ransom, 1985). This supports the contribution of glial cells to $[K^+]_o$ clearance, however also demonstrates the importance of using mature animal models for experimental investigations into $[K^+]_o$ build-up.

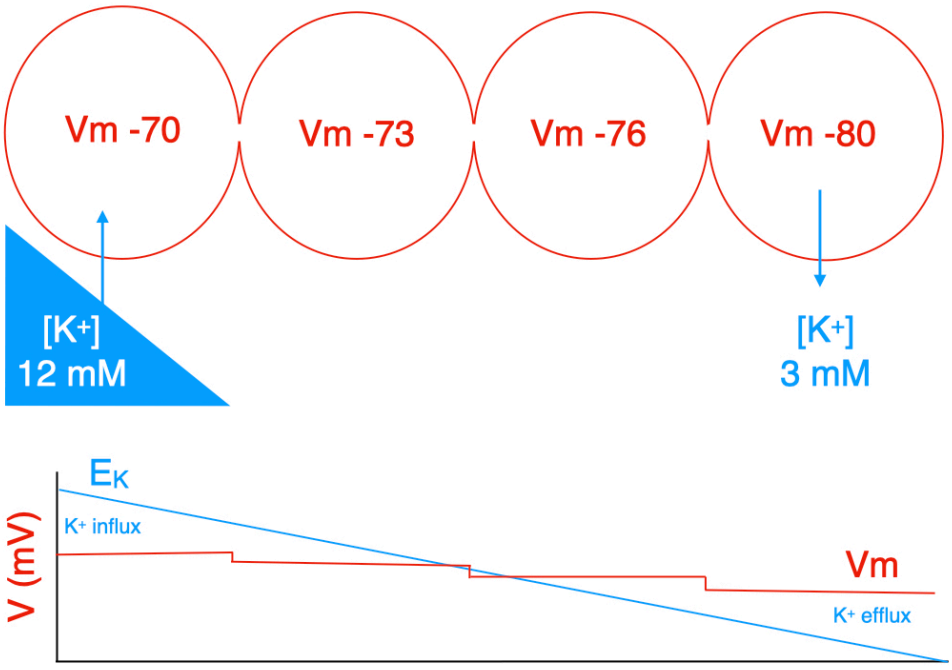

Figure 4.

A schematic demonstrating the process of astrocytic buffering of extracellular K^+ throughout the syncytium via gap junctions. $[K^+]_o$ is elevated at the site of neuronal activity (12mM), resulting in depolarisation of E_K (blue). Astrocytic Vm (red) is negative relative to E_K at the site of activity and thus, Vm is not equal to E_K. As a result, K^+ moves in the direction which drives Vm towards E_K, driving K^+ into local astrocytes via the Na^+/K^+/ATPase, depolarising their membrane. Vm partially moves towards E_K however they are not in equilibrium as only a portion of the membrane is exposed to high $[K^+]_o$. K^+ spreads throughout the syncytium via gap junctions and astrocytes depolarise by a degree determined by the space constant. In the middle cells, Vm becomes more depolarised than E_K, so K^+ effluxes to the next astrocyte, which continues throughout the syncytium *(Hopper, Beswick-Jones and Brown, 2022).*

1.3.3 The Na^+ theory of CAP failure

As $[K^+]_o$ proves unlikely to exceed an $[K^+]_o$ necessary to induce CAP failure during neuronal activity, we must investigate alternative plausible causes. It has been shown that following the cessation of a 100Hz stimulus for 1 second, the post-stimulus recovery of accumulated $[K^+]_o$ follows a double exponential time course, with an initial fast time constant (0.9 ± 0.2s) followed by a later slow time constant (4.2 ± 1s) (Ransom et al., 2000). An attractive interpretation of these findings is that they represent two discrete phases of K^+ clearance from the extracellular space. The fast initial phase is thought to be as a result of K^+ uptake by the Na^+/K^+/ATPase expressed on the surface membrane of glial cells, as we have previously discussed. However, the later sustained phase is alternatively proposed to be via the expression of the Na^+/K^+/ATPase isoform on the axonal membrane (Ransom et al., 2000). This has been shown by a transient undershoot in $[K^+]_o$ from its initial resting concentration of ~3mM to ~2.5mM upon cessation of stimulation (Connors et al., 1982). Importantly, the magnitude of this undershoot appears to increase with increasing stimulus duration (Bay and Butt, 2012). This undershoot is thought to be as a result of axonal Na^+/K^+/ATPase activation, which although considered not to be sensitive to changes in $[K^+]_o$, it is responsive to elevations in intracellular $[Na^+]$ ($[Na^+]_i$), which would begin to rapidly rise during the imposition of a high frequency stimulus (Gordon et al., 1990). Na^+ is therefore rapidly pumped out of the axon in an effort to reduce this accumulation and consequently, extracellular K^+ is co-transported into the axon in conjunction, resulting in the observed reduction of $[K^+]_o$ below baseline.
This activity-dependent $[Na^+]_i$ accumulation would act to reduce the Na^+ reversal potential towards zero, bringing it closer to the axonal resting membrane potential. Consequently, there would exist a reduced electrogenic driving force for Na^+ influx which is responsible for the peak of the action potential. As a result, a reduction in CAP amplitude would be observed during electrophysiological recordings. This has been supported with computational models investigating the effects of high-frequency stimulation on axonal $[Na^+]_i$ accumulation, in both myelinated and un-myelinated axons (Zang and Marder,

2021). This model confirmed that $[Na^+]_i$ accumulates during high-frequency firing, however at a slower rate in myelinated axons than in unmyelinated. This is due to Na^+ diffusing away from the nodes towards the neighbouring juxtaparanodal compartments which act as an 'anti-flood-water reservoir', causing nodal Na^+ to accumulate at a much slower rate (Zang and Marder, 2021). Na^+ then diffuses back towards the node during Na^+ extrusion via the Na^+/K^+/ATPase. Additionally, larger diameter axons were consistently observed to be more robust during the imposition of a high frequency stimulus, compared to those smaller. However, during prolonged periods of high frequency firing, $[Na^+]_i$ accumulation proceed to compromise axonal firing, even in those with larger diameters and thus, greater metabolic capabilities (Zang and Marder, 2021). This therefore suggests that the physical properties of axons do indeed constrain their resilience to high frequency firing due to inter-axonal Na^+ accumulation.

In our study, we aim to experimentally investigate the effects of accumulating $[K^+]_o$ and $[Na^+]_i$ on the CAP profile during the imposition of varying frequency stimulus in MON. It is technically difficult to measure intracellular $[Na^+]_i$ in axons of different size, therefore indirect methods must alternatively be exploited through recordings of extracellular $[Na^+]$ and subsequent mathematical rearrangement of the Nernst equation to calculate ENa and then $[Na^+]_i$.

Chapter 2: Methodology

2.1 Ethics approval

All experiments were approved by the University of Nottingham Animal Care and Ethics Committee and carried out in accordance with the Animals (Scientific Procedures) Act 1986. This was under appropriate authority of establishment, project and personal licences, and conform to the principles and regulations described in the Editorial by Grundy (Grundy, 2015). Experiments were performed on male CD-1 mice (weight 28–35 g, corresponding to 30–45 days of age) purchased from Charles River Laboratories (Margate, UK). Mice were group housed with *ad libitum* access to food and water and maintained at 22–23°C on a 12 h:12 h light–dark cycle. A total of 68 mice were used, with both nerves used for recordings in separate chambers and treated as independent samples. In total 101 optic nerve recordings were made.

2.2 Dissection

Male CD-1 mice were killed by S1 cervical dislocation followed by subsequent decapitation for permanent cessation of circulation and death confirmation. The head was then dissected by making an incision with a scalpel along the skin at the posterior of the head, exposing the skull bones beneath. These were then cut into sections to facilitate their easy removal using small surgical scissors. The skull was cut longitudinally from the base to the nose, with small perpendicular lateral cuts out from this line. Incisions were then made directly behind the orbit of the eye in order to truncate the optic nerves at point in which they exit the eyeball. This was done as close to the orbit as possible in an attempt to retain optic nerve length between 5 – 7 mm. The cerebral hemispheres were then lifted back 180° to expose the optic nerves which were gently freed from their dural sheaths, taking care not to stretch them during this process. Nerves were then

cut at the chiasm, leaving the two distinct optic nerves free for transportation to individual interface perfusion chambers (Medical Systems, Greenvale, NY, U.S.A.) (Stys et al., 1991) for experimental testing.

2.3 Electrophysiology

Within the chambers, nerves were maintained at 37°C using a TC-202A bipolar temperature controller (Digitimer, Welwyn Garden City, UK) and perfused with 10mM glucose artificial cerebral spinal fluid (aCSF) containing the following: 126mM NaCl, 3mM KCl, 2mM $MgSO_4$, 26mM $NaHCO_3$, 1.25mM NaH_2PO_4 and 2mM $CaCl_2$. The chambers were continuously aerated with a humidified gas mixture of 95% O_2/5% CO_2 to maintain pH at 7.45. Suction electrodes were made from single-barrelled glass with the end 5mm bent at a 45° angle and briefly heating the end to melt the glass until a tight fit with the nerve is achieved. Two chlorided wires were then attached, with one entering down the centre of the electrode and the other wrapping around the electrode. Subtraction of the coil response from the wire down the centre of the electrode ensures elimination of some of the electrical noise. Two suction electrodes were then backfilled with aCSF and attached to the proximal and distal ends of the nerve (figure 5), where suction was gently applied in order to slightly pull the end of the nerve up into each electrode, while it is ensured that the electrodes are appropriately distanced apart from each other so that the nerve is not too stretched or slack, as this would affect conduction. The proximal electrode was then used to stimulate the nerve generating a CAP, which was evoked by a 125% supramaximal stimulus (30 μs in duration). The distal suction electrode was used to record the CAPs. Therefore, all recordings were orthodromic. The distal suction electrode was connected to an SR560 low noise preamplifier (Stanford Research Systems, Sunnyvale, CA 94089, USA) where the signal was amplified up to 1000x and filtered at 30 kHz. The differential output was fed into a HumBug Noise Eliminator (Digitimer Ltd, Welwyn Garden City, UK) to remove mains frequency noise (50 Hz). The signal was acquired via an Axon Digidata 1550B

using Clampex 11.3 (Molecular Devices Ltd, Wokingham, Berkshire, UK). Once preparation was complete, nerves were allowed to equilibrate for 30 minutes before any recording commenced. At the end of each experiment, the nerves were lightly crushed between a pair of small forceps while recording was continued in order to kill all axons and prevent action potential firing. These recordings could then be subtracted from the experimental recordings before the nerve was crushed during data analysis in order to remove the stimulus artifact from the results.

In experiments where Na^+ was reduced, equimolar choline chloride was added, and when K^+ was increased, an equimolar reduction in Na^+ was added to maintain osmolarity. The nerve was stimulated at a baseline frequency of 1 Hz unless indicated (Isostim A320, WPI, Sarasota, FL, U.S.A.). Increases in stimulus frequency were applied in continuous, uninterrupted episodes of 10 seconds, where the CAP recorded was the average of all CAPs within this period (e.g., for a 2-minute period of stimulus 12 sequential episodes were imposed).

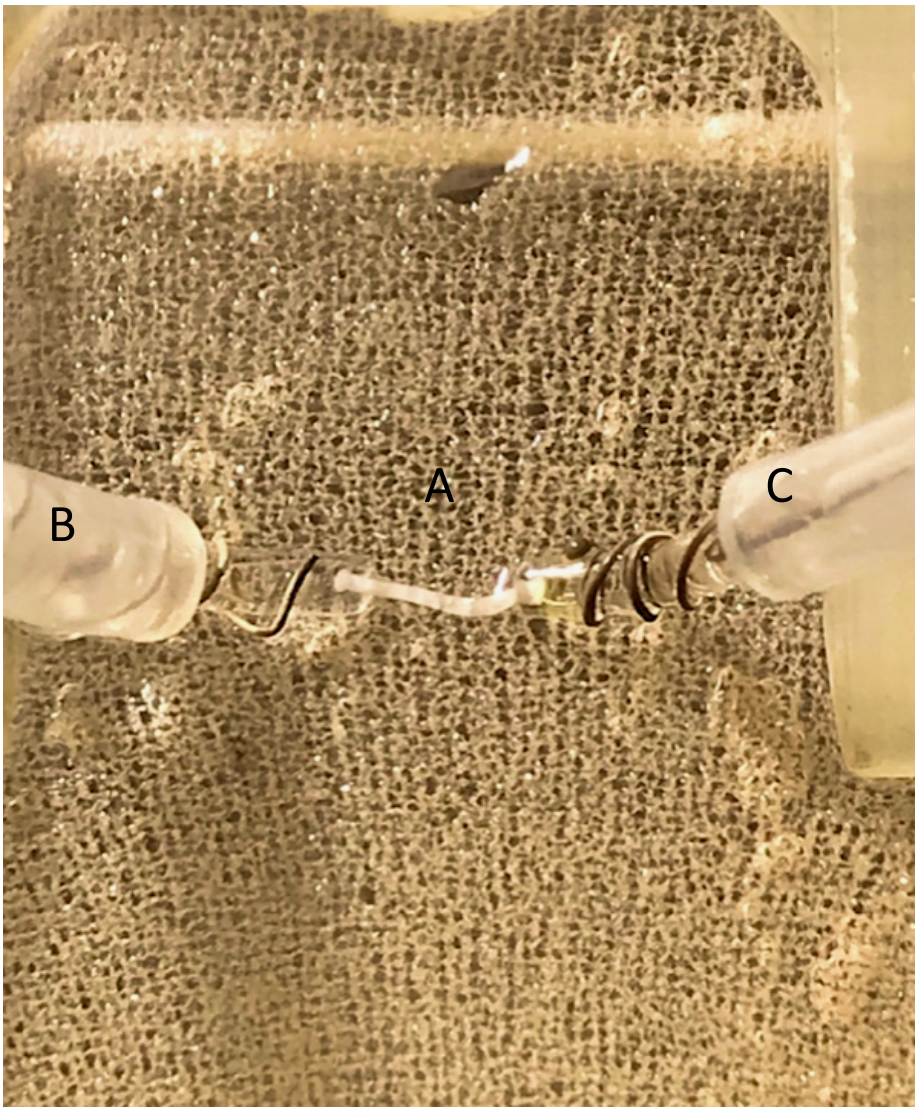

Figure 5.

An image depicting an adult MON within an interface perfusion chamber. The MON is observed (A) between two suction electrodes backfilled with aCSF. The proximal suction electrode (B) is used to stimulate the nerve with a 125% supramaximal stimulus and the distal suction electrode (C) records the subsequent electrical output from all contributing axons within the nerve, observed as a CAP. The nerve is bathed in aCSF solution within the interface perfusion chamber and allowed time to equilibrate before experimental investigation.

2.4 K^+ sensitive microelectrodes

K^+ sensitive microelectrodes permit accurate real-time measurements of $[K^+]_o$, which can be temporarily correlated with an imposed stimulus. Electrodes were fabricated using double-barrelled piggyback glass (WPI, PB150F-6) as previously described (Borrelli, 1985), with slight modifications. The double-barrelled glass was then pulled to a fine tip using a vertical electrode puller (Narishije PC100), as seen in figure 6. The larger ion sensitive barrel was back filled (Microfil 34-gauge tip, WPI) with buffer solution and bevelled while constant pressure was applied via a syringe and tubing: when the solution emerged from the tip it was indicated that sufficient bevelling of the electrode had occurred. This barrel was then back filled with a small volume of N,N-dimethyltrimethylsilyamine (silane) (41716; SigmaAldrich, Merck Life Science UK Ltd, Gillingham, Dorset, UK) and the electrodes were baked at 160°C for 1 hour (Ambiano mini oven, Aldi), permitting evaporation of the liquid silane and the generation of a hydrophobic coat lining the lumen and electrode tip. Once baked, the ion-sensitive barrel was back-filled (Microfil 34-gauge tip, WPI) with 100 mM KCl, 20 mM HEPES adjusted to pH 7.2 with 1 M NaOH and the indifferent barrel was back filled with 150mM NaCl, 20mM HEPES adjusted to pH 7.4 with 1M NaOH. The electrode tip was then inserted into a reservoir of K^+ sensitive ionophore (K ionophore I Cocktail B, 99373, SigmaAldrich) and front filled via suction, such that a column between 100 and 300μm in length filled the tip of the electrode. When the electrode is inserted into the MON (as seen in figure 7), the valinomycin within the resin facilitates the absorption and transportation of K^+ within the extracellular space across the plane, where it is released into the electrode solution. This thereby creates a flow of current.

The ion-sensitive microelectrode was connected to an Axoprobe 1B amplifier via an HS-2 x0.0001 MU headstage and the indifferent (reference) electrode was connected via a HS-2A x0.1 LU headstage. The reference signal was subtracted from the ion-sensitive signal and amplified 10x. This was then fed into a HumBug Noise Eliminator (Digitimer Ltd) to remove main frequency noise (50 Hz). The

signal was acquired via a MiniDigi 1A using Axoscope 11 (Molecular Devices) at 10 Hz.

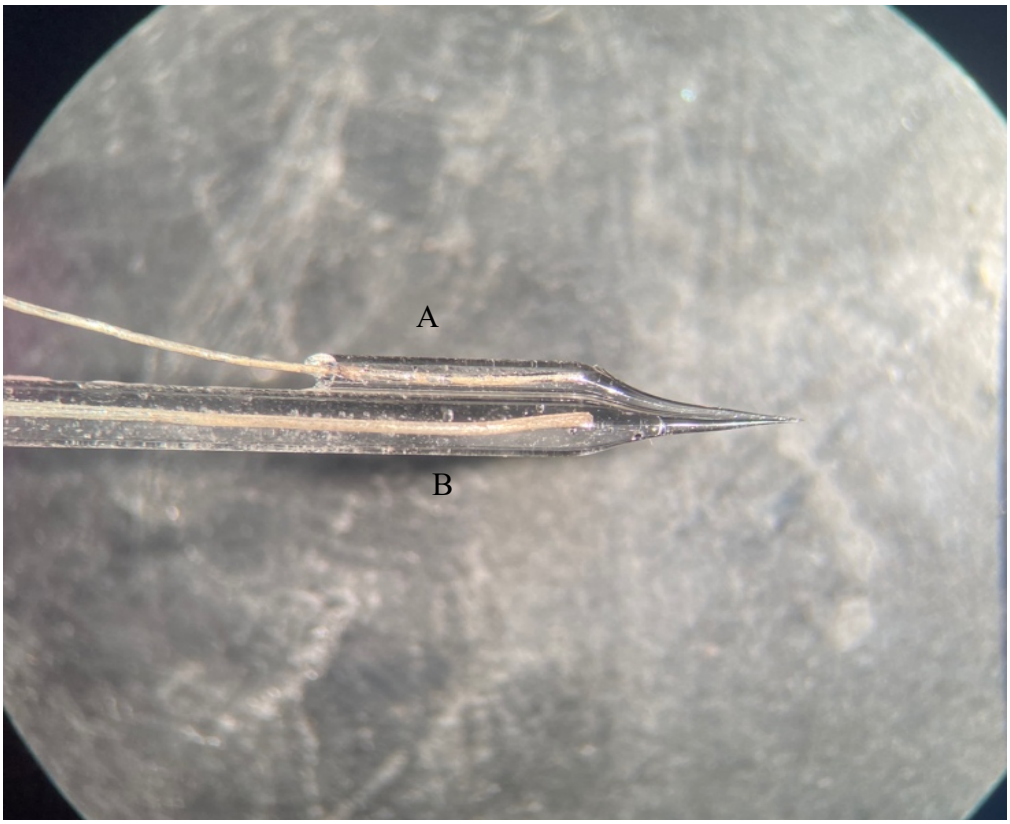

Figure 6.

A double-barrelled K^+ sensitive microelectrode can be seen, pulled to a sharp tip. The smaller indifferent barrel can be seen on top (A) and the larger ion sensitive barrel on the bottom (B).

A B

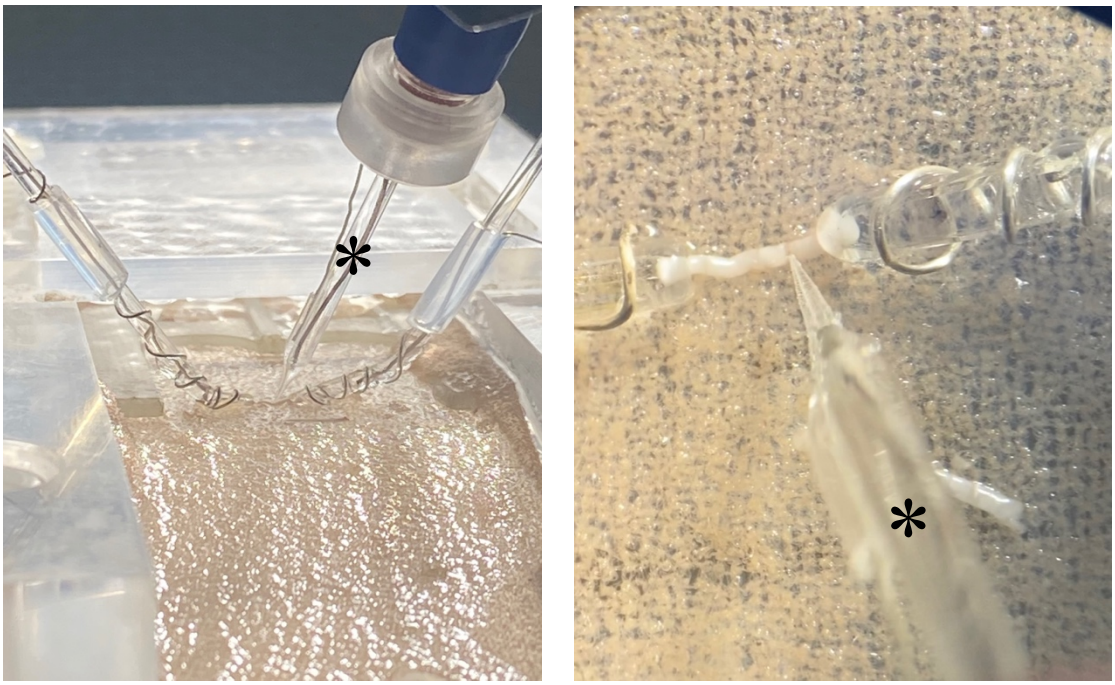

Figure 7.

K^+ sensitive microelectrode setup can be observed (A) and from a closer arial view (B). The microelectrode (indicated *) can be observed inserted into the MON, where the $[K^+]$ within the extracellular fluid can be measured. The MON can be seen to be attached to suction electrodes at the proximal and distal ends, as described in figure 5.

2.5 K^+ Calibration

Fabricated K^+ sensitive microelectrodes were calibrated in a solution containing 120mM NaCl and 20mM HEPES with varying known concentrations of KCl (in mM) 3, 9, 30. These concentrations were selected after taking into careful consideration the implications of the Nernst equation. When superperfused with 3mM KCl, $[K^+]_o$ in *ex vivo* tissue from adult MON is ~3mM. Under physiological conditions, adult MON does not exceed 10mM. Therefore, these are appropriate calibration ranges in order to maximise the signal to noise ratio. A motorised manipulator (EC1 60-0577 control unit with EC1 60-0571 standard motorised control manipulator: Harvard Apparatus) was used for placement of the K^+ sensitive microelectrode in the nerve. All electrodes were individually calibrated and only those showing stable, near Nernstian responses (that is, 50 to 60mV) to decade changes in $[K^+]$ were used for experimental measurements. Electrodes were recalibrated after each experiment and data from electrodes with greater than a 5mV deviation in response to decade changes in $[K^+]$ were discarded. The average between the initial and final calibrations was used to evaluate experimental data. The $[K^+]_o$ was estimated using the following rearrangement of the Nernst equation:

$$[\mathrm{K}]_\mathrm{o} = 3\mathrm{mM} \times 10^{\left[\frac{\mathrm{V}}{\mathrm{slope}}\right]}$$

where V is the differential output from the amplifier in mV and slope is the electrode response to a decade change in K^+ from 3 mM to 30 mM in mV. Post experimental calibrations and data manipulations were carried out using Microsoft Excel (Microsoft).

2.6 Curve fitting and data analysis

The triphasic CAP was analysed using Clampfit 11 (Molecular Devices). The area under the CAP during a supramaximal stimulus was used as a quantitative measure of axon function within the optic nerve. This is because the CAP is considered as the summed currents of all conducting axons within the nerve tract (Stys et al., 1991).

Measurement of the amplitudes of the individual peaks were complicated by the superimposition of the second CAP peak on the first peak. Therefore, amplitude measurements of the first peak contained considerable contribution from the second peak. The second and third CAP peaks however did not significantly superimpose, therefore allowing straightforward amplitude measurements to be obtained. The first peak area was measured using a Gaussian fit and converted to an amplitude to eliminated interference from the second peak, according to:

$$\mathrm{Amp} = \frac{\mathrm{Area}}{\mathrm{w\ x}\sqrt{\frac{\pi}{2}}}$$

where w is the width of the peak.

2.7 Calculation of $[Na^+]_i$

$[Na^+]_i$ was calculated using indirect methodology, since real-time absolute concentrations are impossible to measure directly in such small axons. To do this, extracellular $[Na^+]$ was decreased in the aCSF bathing the nerves, resulting in a corresponding decrease in CAP amplitude during stimulation. The CAP amplitude was normalised and expressed as a percentage, so when at baseline equalled 100%. This concentration dependent fall in CAP was then calibrated against the extracellular $[Na^+]$ on a logarithmic scale, producing an explicit equation. Rearrangement of the Nernst equation and simultaneous equations as described by Brown, 2020, were then used to estimate changes in $[Na^+]_i$ during the imposition of a stimulus as seen:

$$CAP = 107.998\ log_{10}\ [Na]_o - 134.33$$

$$\downarrow$$

$$E_{Na} = 0.57\ CAP + 14.99$$

$$\downarrow$$

$$[Na]_i = \frac{155}{10^{\frac{E_{Na}}{61.5}}}$$

We used simultaneous equations for estimations of $[Na^+]_i$ in similar manner to that used by Hodgkin and Huxley (1952a), to quantify the leak current.

Chapter 3: Results

3.1 The effects of increasing stimulus voltage on CAP recruitment

It was proposed by Allen et al (2006), that the triphasic profile of the CAP is generated by three distinct sub-populations of axon diameter, with the largest axons contributing to the first peak, intermediate sized to the second peak and smallest to the third. Electrophysiological experiments could be used to indirectly investigate this by progressively increasing the stimulus voltage imposed upon the MON in increments, in order to determine the recruitment of each of the three CAP peaks. It can be observed from figure 8, that stimulating the MON at increasing stimulus voltages recruited the 3 peaks of the CAP in a sequential manner. The first peak was recruited at the lowest stimulus intensity, followed by the second and third peaks, respectively (figure 8).

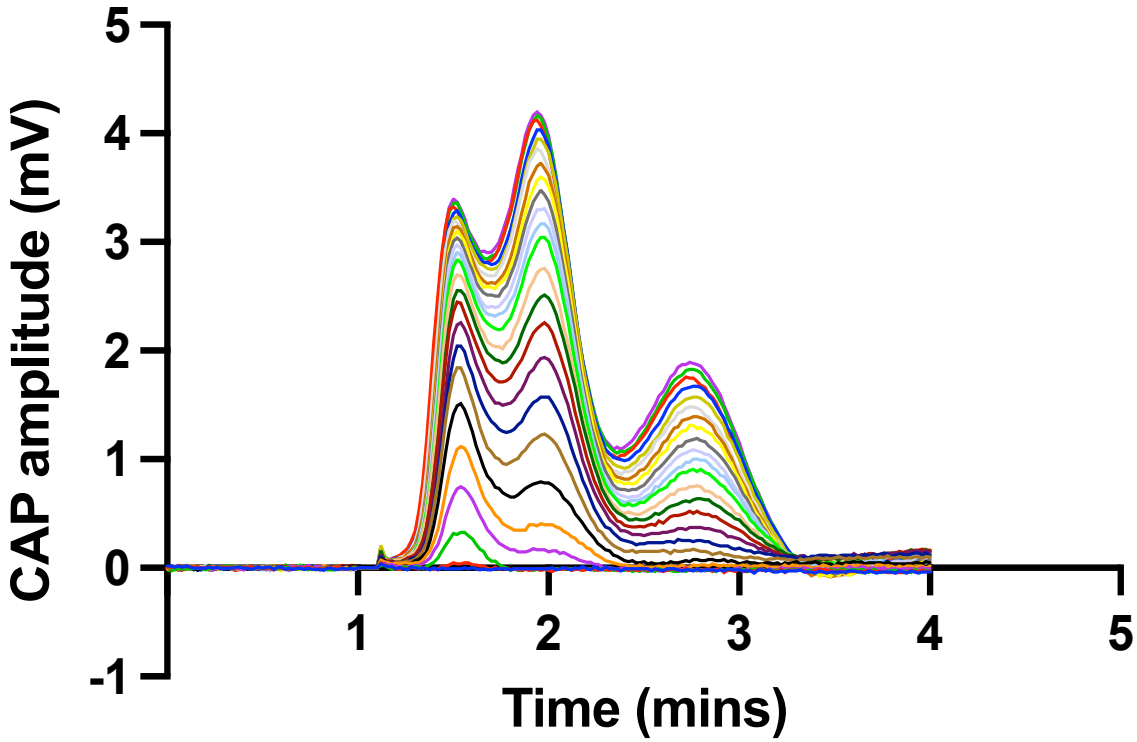

Figure 8: *Recruitment of the three CAP peaks during increasing stimulus voltage.*

The three peaks of the CAP can be observed to be recruited in a sequential manner as stimulus voltage (V) is progressively increased. The first peak is recruited at the lowest stimulus intensity and therefore first, followed by the second and third peaks, respectively. A 30 μs stimulus was applied at 1 ms.

The area for each peak at increasing stimulus voltage was then converted to a cumulative histogram (figure 9), showing the cumulative distribution of the areas of the individual CAP peaks. It can be again observed that the first peak is fully recruited at the lowest stimulus intensity of ~5V, with the steepest rate of rise. Stimulus voltage must then reach ~8V before the second peak reaches full recruitment, followed by the third peak which demonstrates the highest stimulus threshold for recruitment (~12V).

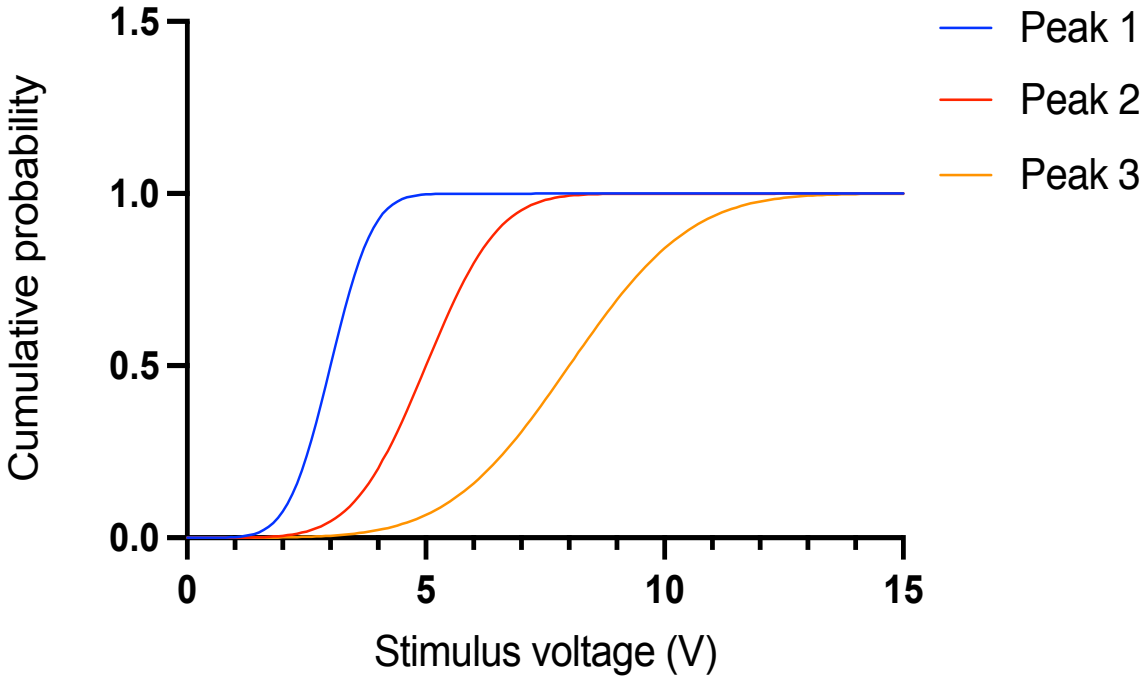

Figure 9: A cumulative histogram plot showing the cumulative distribution of the three CAP peaks during increasing stimulus voltage.

The cumulative distribution of the three CAP peaks can be seen during increasing stimulus voltage (V). The first peak (blue trace) can be seen to be recruited at the lowest stimulus voltage (~5V), followed by the second peak (red trace) at ~8V and then the third peak (orange trace) at the highest stimulus intensity (~12V).

Fitting the area of each peak from figure 9, with a Gaussian curve could then produce values for the mean ± standard deviation (SD), which could be utilised to generate Gaussian normal distributions for each of the three peaks (figure 10).

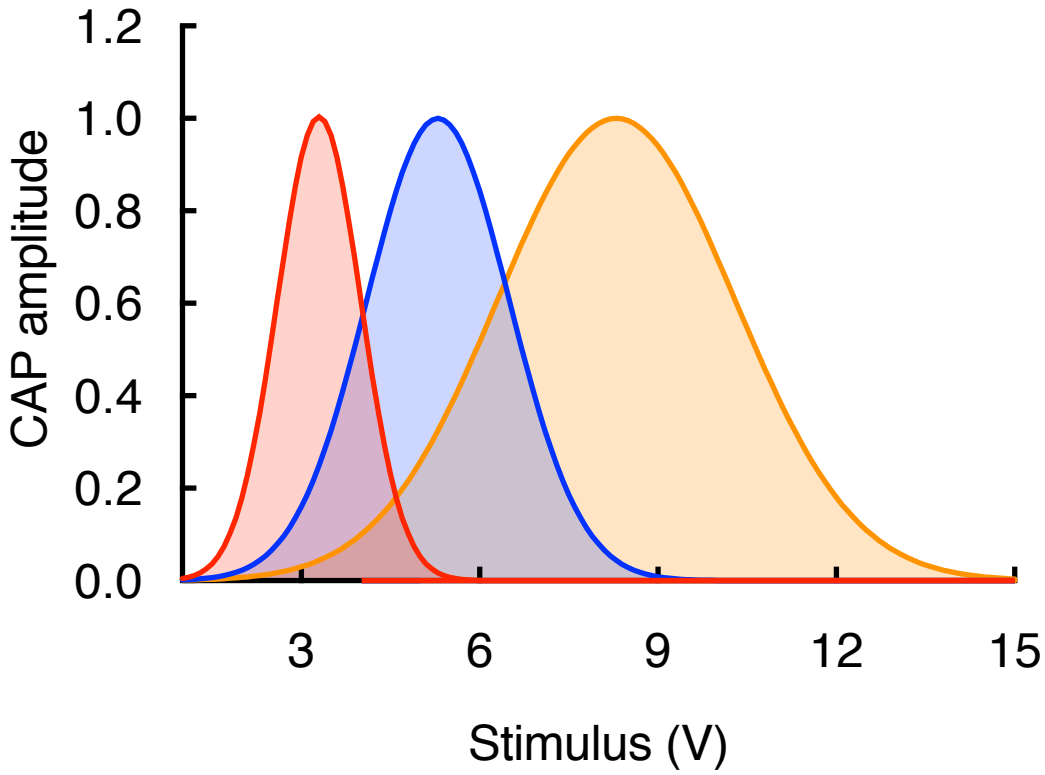

Figure 10: Gaussian distribution for each of the three CAP peaks.

Gaussian distributions for each of the three CAP peaks were generated using mean ± SD values generated from fitting the area of each peak from figure 9 with a Gaussian curve.

When this Gaussian distribution is superimposed with a CAP, it can be seen that the two profiles look almost identical. This data suggests that the axons contributing to the first peak comprise those with the lowest threshold for activation, known to be thicker fibres with lower axoplasmic resistance. Conversely, axons contributing to the third peak comprise those with the highest threshold for activation, considered as axons with a thinner diameter and higher axoplasmic resistance. It must be noted that the second peak superimposes upon the first peak, leading to significant contribution to the first peak amplitude. This was accounted for by measuring the area of the first peak which was then converted to amplitude, as described in the methodology.

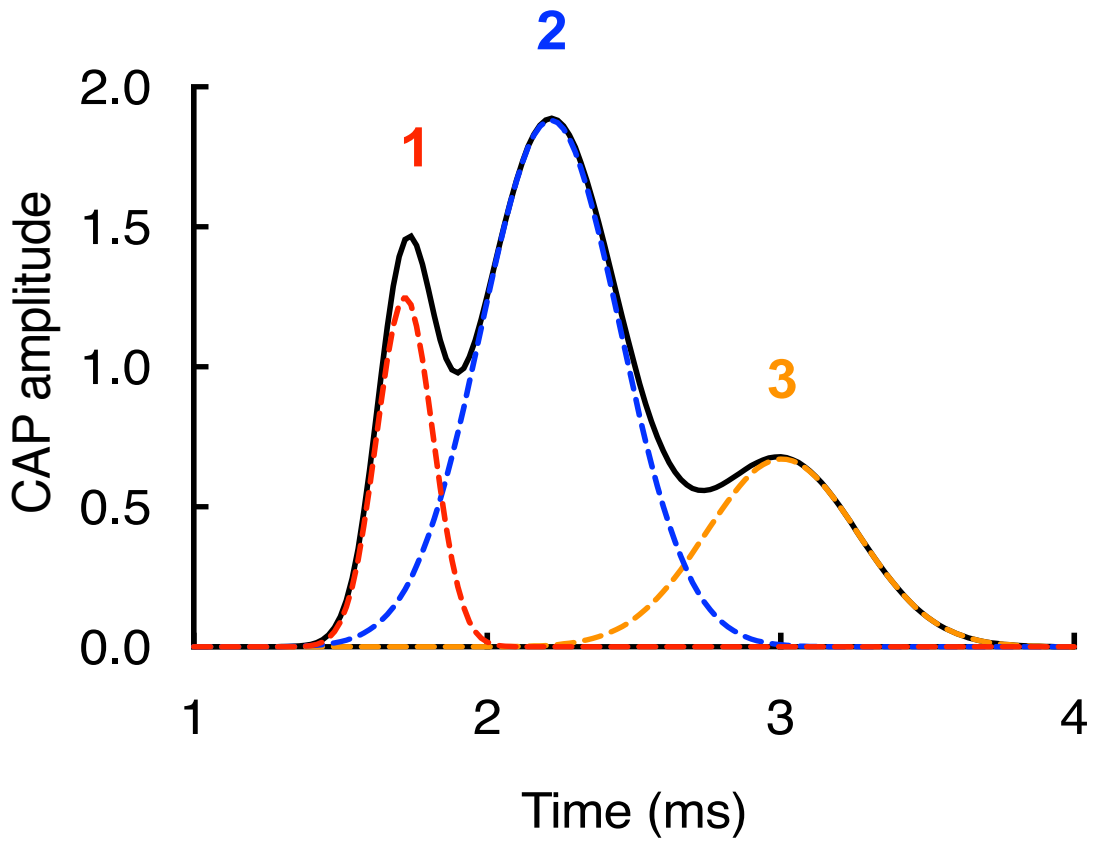

Figure 11: Gaussian distribution fit to the area of the three CAP peaks.

The area of the three CAP peaks during supramaximal recruitment can be fit by a Gaussian distribution.

3.2 The effects of reducing the time interval between frequency stimulations.

As the MON is stimulated, K^+ is extruded into the extracellular space during the repolarising phase of the action potential (Hodgkin and Huxley, 1953). It must therefore be ensured that the time interval between stimulations is sufficient for the refractory period to conclude and that a loss of CAP amplitude is not as a result of Na^+ channel inactivation. This inactivation would consequently reduce the number of channels available for Na^+ to move through and therefore decrease the rate of membrane depolarisation, in addition to CAP peak amplitude, as determined by ENa. Therefore, a double pulse protocol was implemented whereby the interval duration between stimulations to the MON was progressively decreased (from 30 ms to 20, 15, 10, 8, 6, 5, 4, 3 and 2 ms). It was observed that decreasing the stimulation interval down to 5 ms (200 Hz) had a negligible effect on CAP amplitude across all three peaks. Therefore, the second peak was used for illustration (figure12). This suggests that the observation of a fall in CAP amplitude during increased frequency stimulation or altered ionic composition would not be as a result of the duration between stimulations, but alternatively another variable.

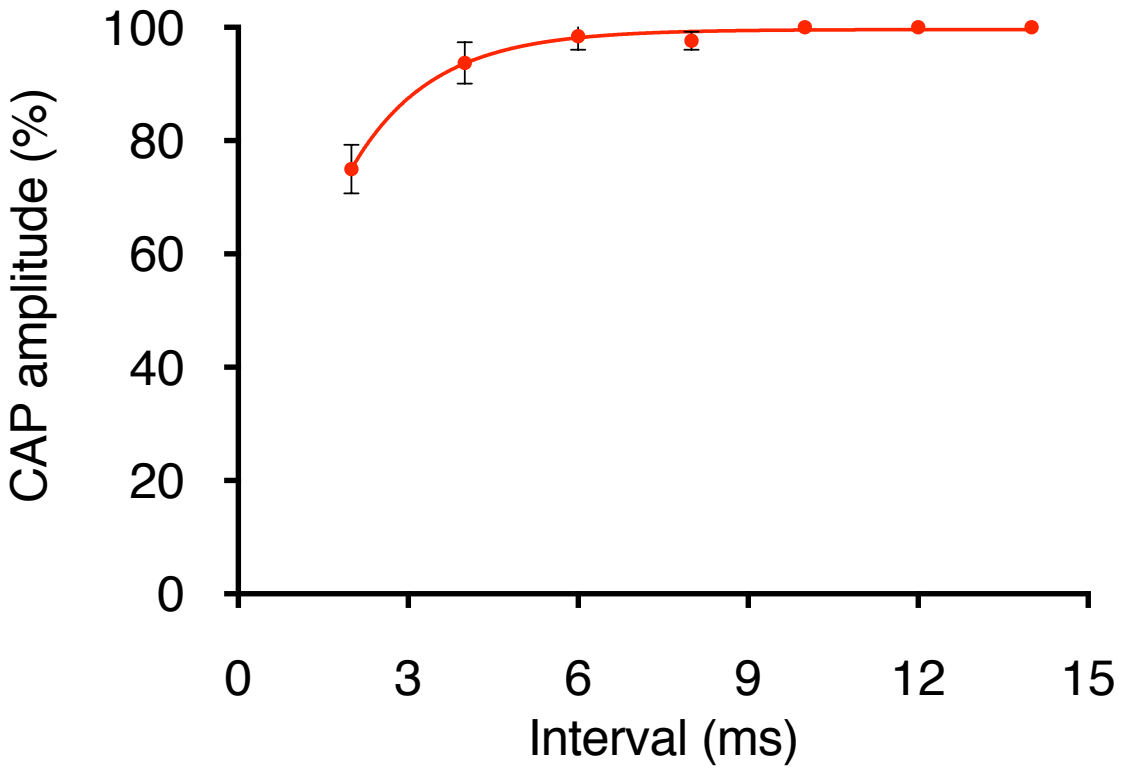

Figure 12: A double pulse protocol at 100 Hz.

The CAP amplitude can be observed during the imposition of a 100 Hz stimulus, as the interval between the next stimulus impulse is decreased from 30 ms to 20, 15, 10, 8, 6, 5, 4, 3 and 2 ms. As the duration between stimulation is decreased, the amplitude of the CAP can be observed to be affected to a negligible extent. During a 4 ms interval between stimulations, the CAP amplitude was observed to fall only 6.2% (SD = 3.7). SD is represented by the vertical bars above and below each data point.

To further investigate the effects of a double pulse protocol on the recruitment of the three peaks, MONs were stimulated once at a lower stimulus voltage and immediately again at a higher voltage. It can be seen in figure 13, that during the first low intensity stimulation, only the first peak of the CAP is recruited, as we would expect from figures 8 and 9. When stimulated again immediately after the first impulse with a second at a higher stimulus intensity, only the second and third peaks were recruited. It would be expected that if the larger first peak axons contributed to these peaks during the second stimulation, their amplitude would be decreased, however this is not observed. This therefore suggests that all axons contributing to the first peak of the CAP were inactivated during the first impulse and were unable to be recruited during the second stimulation. During a separate experiment, MONs were only stimulated once at the higher stimulus voltage where it can be seen that all three peaks of the CAP were recruited. This therefore suggests that each axon only contributes to one individual peak.

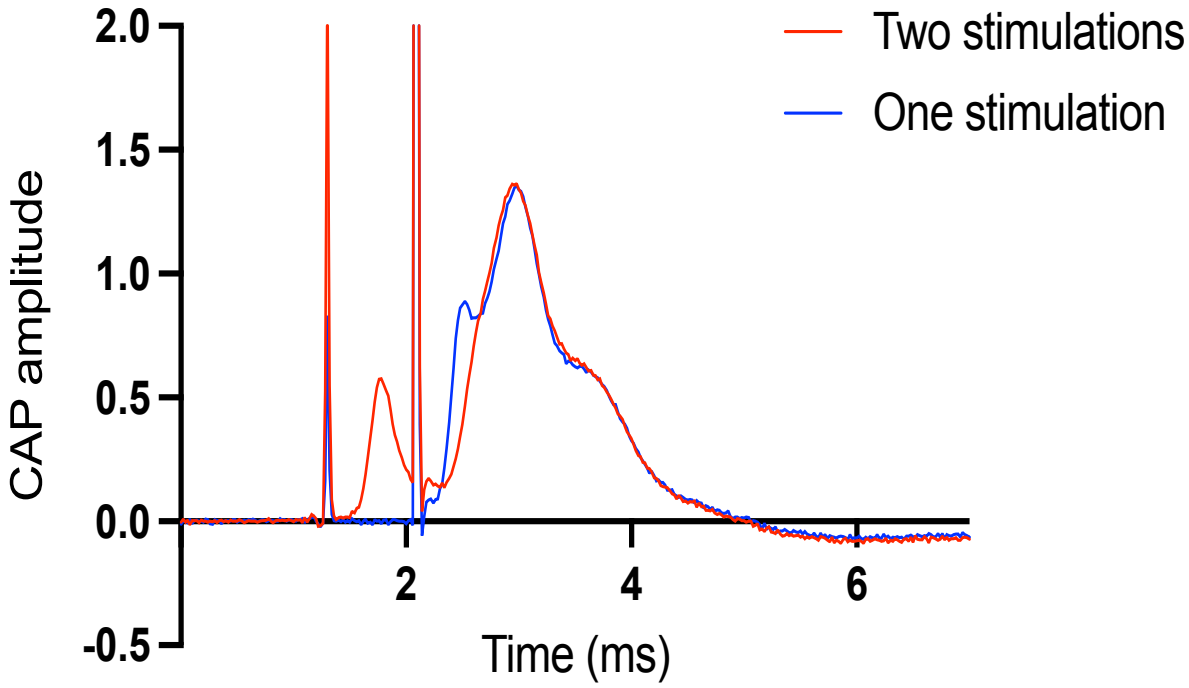

Figure 13: The effects of a double pulse protocol compared to a single stimulation.

When the MON is stimulated at a low stimulus intensity (indicate by the first red peak following the first stimulus artifact), only the first CAP peak is recruited. If immediately stimulated again at a higher stimulus voltage, only the second and third peaks were recruited (red trace following the second stimulus artifact). If the MON was only stimulated once at the higher stimulus intensity, all three peaks of the CAP were recruited (blue trace).

3.3 The response of the three CAP peaks to varying stimulus frequency.

It can be appreciated that a supraphysiological frequency stimulation to the MON increases its metabolic demand in order to sustain high frequency firing. At the point in which the axonal metabolic supply and demand are in disequilibrium, a fall in the CAP amplitude would be expected due to insufficient ATP supply for the redistribution of transmembrane ion concentration gradients after action potential firing. However, the extent to which axon sub-populations maintain their amplitude and profile under such conditions occurs in a differential manner. We tested both 'low' (figure 14) and 'high' (figure 15) frequency stimulations on the MON in order to investigate this. During the imposition of low supraphysiological frequency stimulations to the MON, from the physiological frequency of 5 Hz up to 10, 15, 20 and 30 Hz, a progressive fall in amplitude of all three CAP peaks can be observed, however to different extents (figure 14). The first peak can be observed to remain the most robust throughout increased frequency stimulation, maintaining its amplitude even up to 30 Hz. The second peak exhibits a fall in amplitude beginning at 15 Hz, which progressively increased with frequency stimulation, falling up to ~15% in amplitude at 30 Hz from its baseline stimulation. The third peak is the most affected by increasing frequency stimulation, falling at all tested supraphysiological frequencies. During a 30 Hz stimulus, the third peak can be seen to fall a total of ~47% in amplitude from its baseline, suggesting the axons within this sub-population are the most metabolically sensitive to high frequency firing.

3.3.1 The effects of low frequency stimulation on CAP amplitude.

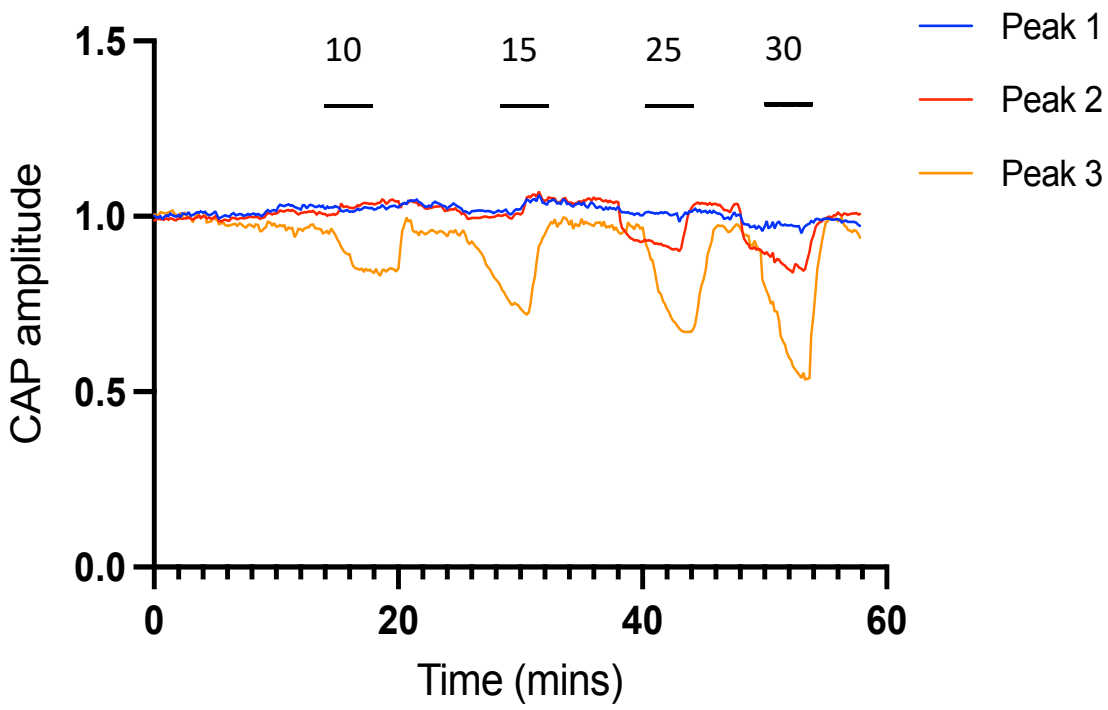

Figure 14: The effects of increasing low stimulus frequency on the amplitude of the CAP three peaks.

Increasing frequency stimulations were imposed upon the MON for 4 minutes, from the physiological frequency of 5 Hz, up to 10, 15, 25 and 30 Hz (as indicated by the bars above each stimulation). The first peak (blue trace) was the most resistant to increasing frequency stimulation, maintaining its amplitude at all frequencies tested (n = 11). The second peak (red trace) begins to progressively fall in amplitude during increasing frequency stimulation, beginning at 15 Hz and falling a total of ~15% in amplitude compared to baseline by 30 Hz stimulation (n = 4). The third peak (orange trace) is the least resistant to increasing frequency stimulation, falling in amplitude at all tested frequencies (n = 12). At 30 Hz, the third peak fell the most out of all three of the CAP peaks, decreasing 47% in amplitude from its baseline (n = 5).

3.3.1The effects of high frequency stimulation on CAP amplitude.

We then investigated the effects of high frequency stimulation on the amplitude of the MON CAP three peaks. Frequency stimulation was progressively increased from the physiological frequency of 5 Hz up to 40, 67, 80 and 100 Hz. It can be seen in figure 15 that increasing the frequency stimulus affected all three of the CAP in a frequency dependent manner, however to different extents. As seen in figure 14, the first peak amplitude was the most resistant to increasing frequency stimulation, however, did exhibit a fall at all tested frequencies. At 100 Hz, the first peak fell ~17% in amplitude from its baseline, inferring metabolic strain on these larger diameter axons. The second peak also progressively fell in amplitude at all frequency stimulations, however to a greater extent than the first peak. At 100 Hz stimulation, the second peak can be observed to fall ~63% in amplitude from its baseline. The third peak however, composed of the smallest diameter axons within the MON is observed to be the least resistant to high frequency stimulation out of all three peaks, significantly falling in amplitude at all tested frequencies. During a 100 Hz stimulus, the third peak fell ~88% in amplitude, indicating drastic changes in the transmembrane ion concentration gradients within this axon sub-population, which cannot be re-equilibrated at this frequency by their metabolic supply.

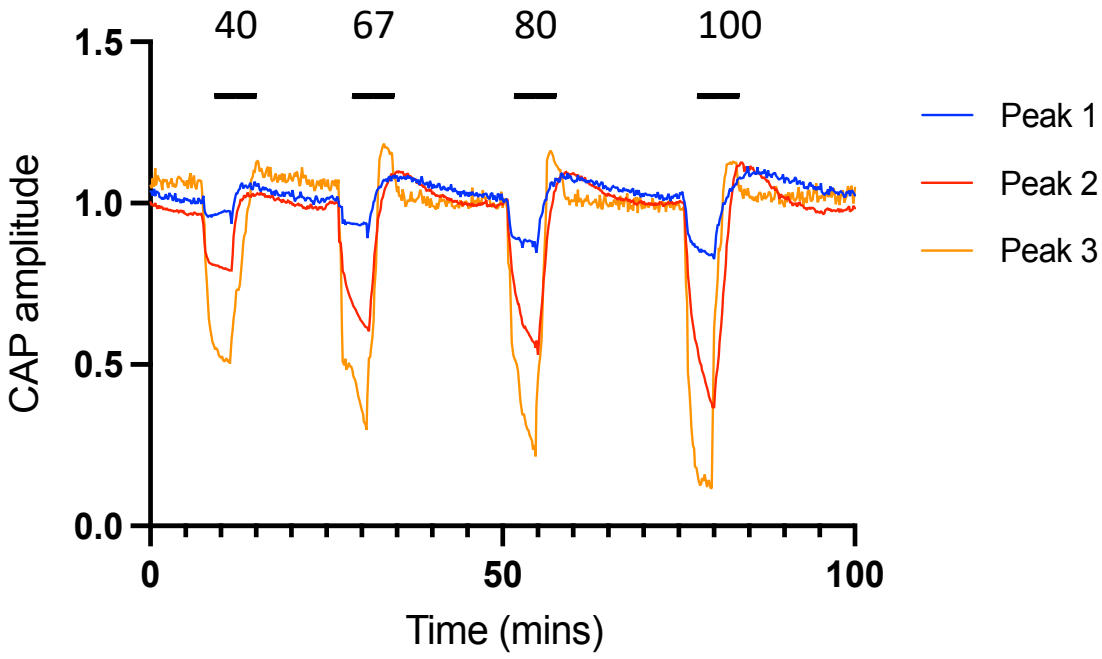

Figure 15: The effects of increasing high stimulus frequency on the amplitude of the CAP three peaks.

The amplitudes of the CAP three peaks can be seen during exposure to increasing frequency stimulations from the physiological frequency of 5 Hz, up to 40, 67, 80 and 100 Hz (as indicated by the bars above each stimulation). Peak 1 (blue trace) was the most resistant of the peaks to high frequency stimulation, progressively decreasing in amplitude at all frequencies (n = 11), however by only ~17% at 100 Hz (n = 9). Peak 2 (red trace) was intermediately resistant, falling by ~63% in amplitude at 100 Hz (n = 10). Peak 3 (orange trace) can be observed to have the greatest fall in amplitude during all stimulus frequencies (n = 11) and fell by ~88% at 100 Hz (n = 10).

The effects of increasing stimulus frequency on the amplitude of the three CAP peaks can be further reinforced in figure 16, which displays all tested stimulus frequencies (Hz) on a logarithmic scale, against CAP amplitude. It can be seen that the first peak is the most robust at maintaining its amplitude during increasing frequency stimulations out of the three peaks, falling only 30.5% at 100 Hz. Conversely, the third peak is the most sensitive to increasing stimulus frequency, exhibiting the most drastic fall in amplitude at all tested frequencies. At 100 Hz stimulation, the third peak fell 83.6%.

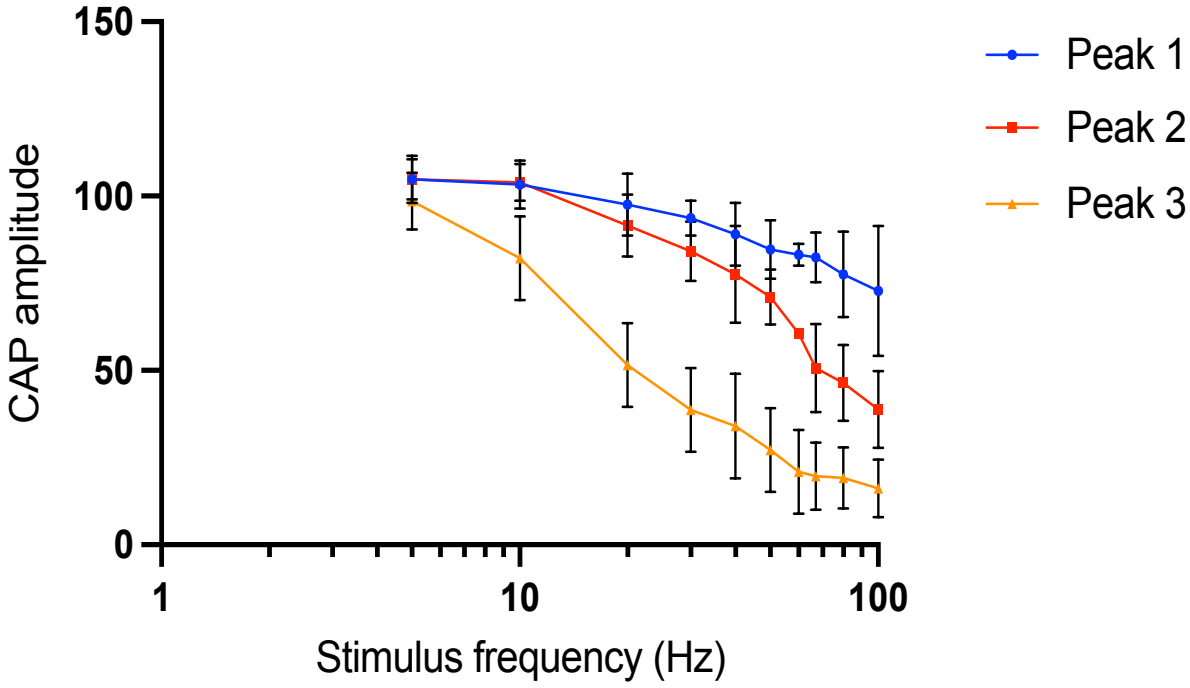

Figure 16: The effects of increasing stimulus frequency on a log_{10} scale on the amplitude of the three CAP peaks.

As stimulus frequency increases, all three peaks of the CAP begin to progressively fall in amplitude. The first peak (blue) can be observed to be the most robust to withstanding high frequency stimulus, falling only 30.5% (SD= 18.6) in amplitude at 100 Hz (n= 9). The second peak reduces in amplitude by 63.0% (SD= 11.0) at 100 Hz (n = 10) and the third peak can be observed to be affected the most by increasing frequency stimulus, falling 83.6% (SD= 8.2) at 100 Hz (n = 10). Standard deviation (SD) is represented by the vertical bars above and below each data point.

Under physiological conditions, the axonal Na^+/K^+/ATPase maintains an $[Na^+]_i$ of ~10mM (Ransom et al., 2000). This provides a steep concentration gradient and driving force for Na^+ to rapidly influx into the axon during the depolarising phase of an action potential. We would predict that during high frequency stimulation to the MON, $[Na^+]_i$ would begin to increase due to Na^+ influx through Na^+ channels. If the rate of Na^+ influx exceeds the capacity for the axonal Na^+/K^+/ATPase to move intracellular Na^+ out of the axon, then an accumulation of $[Na^+]_i$ would be expected in a frequency dependent manner. This elevation in $[Na^+]_i$ would then decrease ENa as the extracellular $[Na^+]$ remains unchanged at the physiological concentration of 155 mM. The ratio of $[Na^+]_o$: $[Na^+]_i$ will decrease causing ENa to fall towards 0mV. Consequently, a fall in CAP amplitude and rate of rise would be expected.

However, absolute real-time measurements of $[Na^+]_i$ cannot be accurately measured though direct methods, creating difficulties to investigate this. Therefore, indirect methods must alternatively be utilised to our advantage in order to predict such measurements. The logic is such that a fall in CAP amplitude and rate of rise during the imposition of a high frequency stimulus, as predicted by a fall in ENa, can be mimicked through manual reductions in the $[Na^+]$ within the aCSF bathing the nerves. This will decrease the transmembrane $[Na^+]$ gradient across the nerve and therefore decrease ENa which can be calculated as $[Na^+]_i$ is assumed to remain unchanged. The quantitative results of reducing extracellular $[Na^+]$ on CAP profile can then be analysed through manipulation of the Nernst equation as described in the methodology section and used to estimate the increase in $[Na^+]_i$ during high frequency stimulation when $[Na^+]_o$ remains unchanged.

During a decrease in $[Na^+]_o$ in the aCSF from the physiological concentration of 155 mM to 100, 80, 60, 50, 40 and 30 mM, a progressive fall in CAP amplitude is observed (figure 17), since ENa will decrease, in addition to an increase in latency. This reduction in amplitude can be observed to be most pronounced at the lowest extracellular $[Na^+]$ investigated (30 mM) (figure 17).

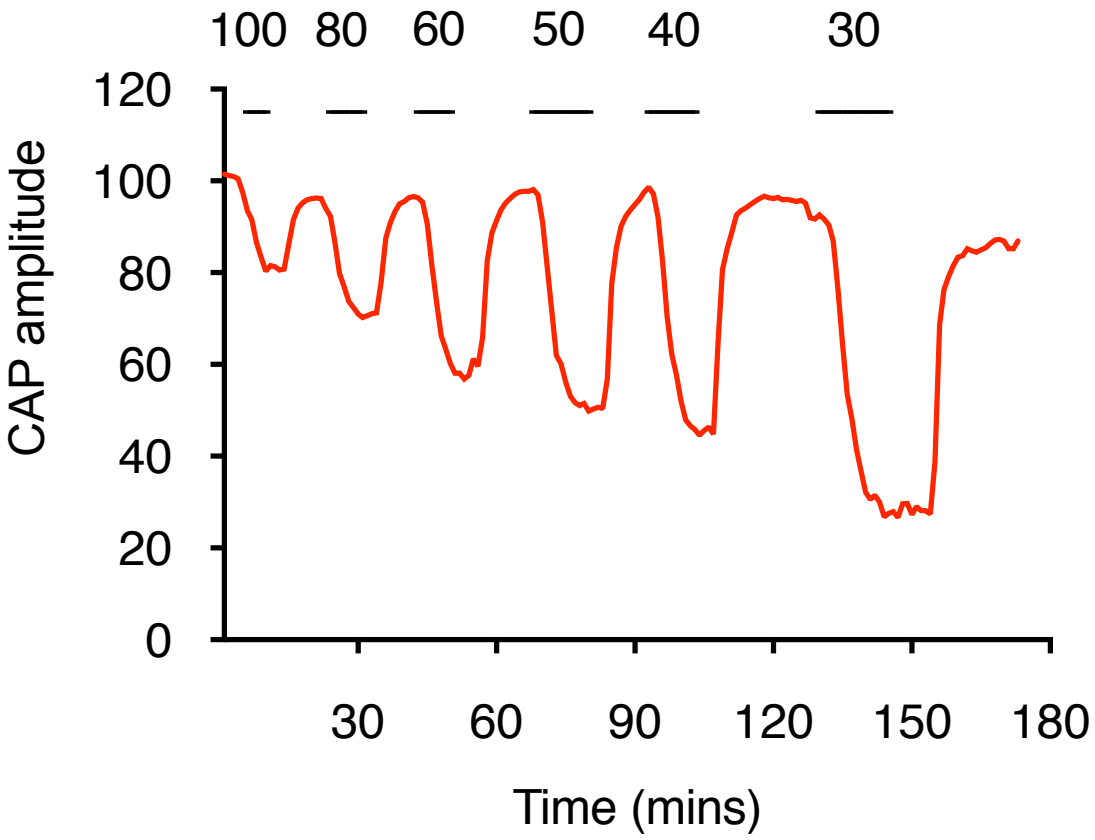

Figure 17: The effects of reducing $[Na^+]_o$ on CAP amplitude.

As the $[Na^+]$ in the aCSF bathing the MONs is decreased from the physiological concentration of 155 mM down to 100, 80, 60, 50, 40 and 30 mM (as represented by the bars above each stimulation), there is a progressive fall in the CAP amplitude during a supramaximal stimulation (n = 12). This decrease in CAP amplitude is in a concentration dependent manner, with the greatest decrease in amplitude observed at 30mM $[Na^+]_o$ (n = 4)

This fall in CAP amplitude during decreasing $[Na^+]_o$ occurred in a uniform manner across all three of the CAP peaks, which fell to the same extent. This is thought to be due to the same $[Na^+]$ within the aCSF bathing all of the axons within the MON, which therefore has a generalised effect on ENa across all axons. The second peak was therefore selected for illustration (figure 18) and its amplitude was plotted against $[Na^+]_o$ on a logarithmic scale. Standard deviations were calculated for each data point and an equation was then generated showing a linear relationship. This equation could later be used for estimations of ENa and $[Na^+]_i$.

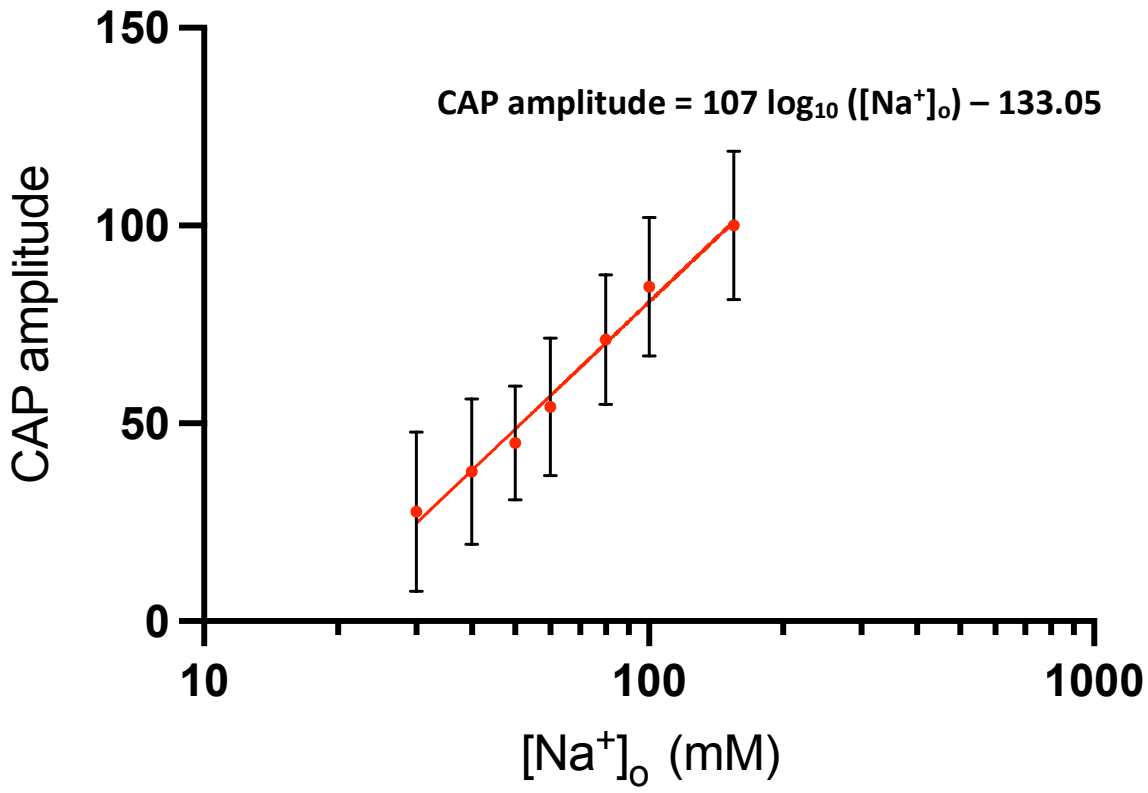

Figure 18: The effects of decreasing extracellular $[Na^+]$ on CAP amplitude.

CAP amplitude of the second peak is plotted against $[Na^+]_o$ on a logarithmic scale (log_{10}). The CAP falls in a concentration dependent manner with $[Na^+]_o$ (n = 12) which was fit with a linear regression and equation of the line, showing a linear relationship. SD were calculated for each data point (seen as the vertical bars above and below each data point).

The equation generated from figure 18 could then be used to solve for estimations of ENa and then $[Na^+]_i$ through manipulation of the Nernst equation, as described in the methodology section. Calculated values for ENa and $[Na^+]_i$ were then plotted against stimulus frequency (figure 19), where ENa can be observed to decrease with increasing frequency, as $[Na^+]_i$ increases towards a maximal concentration of ~40mM at 100 Hz. ENa and $[Na^+]_i$ appear to mirror each other, reflecting how ENa contributes to the value of $[Na^+]_i$.

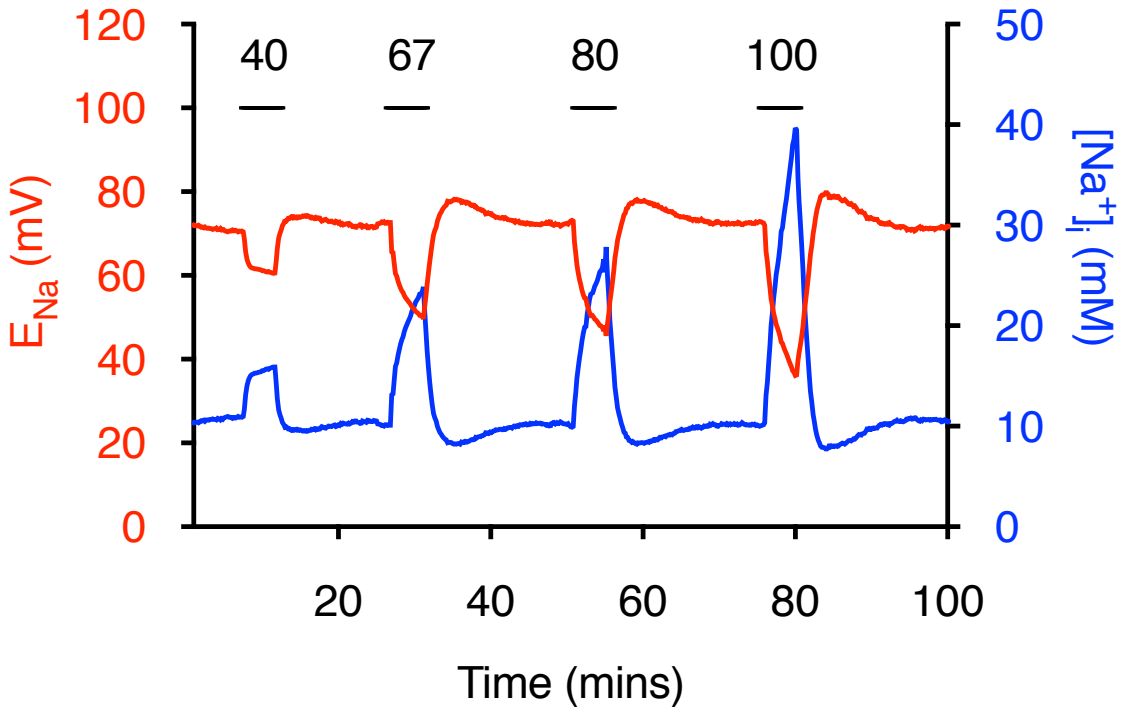

Figure 19: Calculated values for ENa and intracellular $[Na^+]$.

Values for ENa (blue trace) and $[Na^+]_i$ (red trace) were calculated from the data shown in figure 18, using manipulation of the Nernst equation. In the second peak as $[Na^+]_i$ (mM) increases, ENa (mV) decreases. These effects can be seen to mirror each other.

When stimulus frequency is plotted on a logarithmic scale, it can be seen that as the frequency is increased from the physiological frequency of 5Hz up to 10, 20, 30, 40, 50, 60, 67, 80 and 100 Hz, $[Na^+]_i$ increases in all three peaks of the CAP, however in a differential manner. It can be observed in figure 20 that the axons contributing to the third peak of the CAP are the most prone to accumulating intracellular Na^+ as stimulus frequency is incrementally increased, with the steepest rate of rise. At 100 Hz stimulation, the third peak accumulates 62.9 mM $[Na^+]_i$. The axons contributing to the second peak of the CAP are seen to accumulate $[Na^+]_i$ to an intermediate extent as stimulus frequency is increased, with an $[Na^+]_i$ value of 44.7 mM at 100 Hz. The axons contributing to the first peak have the most gradual elevations in $[Na^+]_i$ with increasing stimulus frequency, shown to accumulate to 22.3 mM at 100 Hz stimulation.

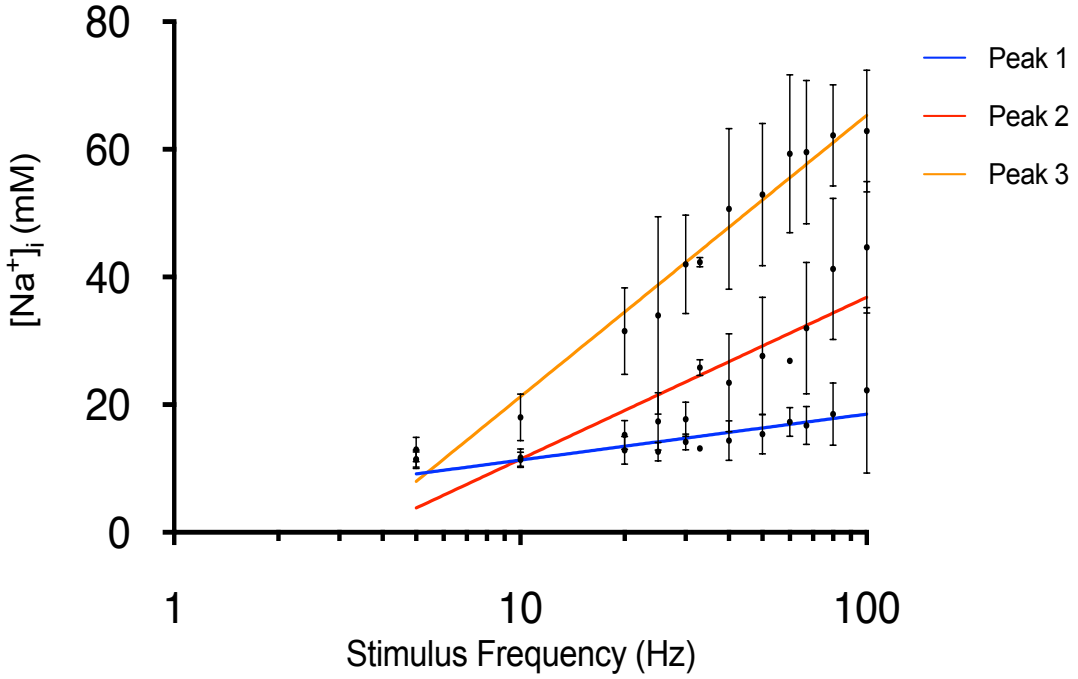

Figure 20: The effects of increasing stimulus frequency on calculated intracellular [Na^+].

Increasing stimulus frequency (Hz) was plotted on a $\log_{10}$ scale against calculated values for $[Na^+]_i$. As the stimulus frequency is increased from the physiological frequency of 5 Hz up to 10, 20, 30, 40, 50, 60, 67, 80 and 100 Hz, $[Na^+]_i$ increased in axons contributing to all three of the CAP peaks, however to different extents. The first peak (blue trace) is the most resistant to $[Na^+]_i$ accumulation increasing from ~11 mM at 5 Hz stimulation (n = 7), up to 22.3 mM (SD = 13.0) at 100 Hz (n = 15). In the second peak (red trace), $[Na^+]_i$ increases from ~11 mM (5 Hz) (n = 7) up to 44.7 mM (SD = 10.3) at 100 Hz (n = 16) and the third peak (orange trace) is the most sensitive to high frequency stimulation, increasing $[Na^+]_i$ from ~13 mM at 5 Hz (n = 7), up to 62.9 mM (SD = 9.5) (100 Hz, n = 15). SD is calculated, shown as the vertical bars above and below each data point.

3.5 The effects of increased $[K^+]_o$ on CAP amplitude.

We have predicted in section *3.4* that during high frequency stimulation, $[Na^+]_i$ accumulates up to ~60 mM. However previous published data suggests that $[K^+]$ liberated from the axon during neuronal activity can accumulate within the extracellular space (Ransom et., 2000) and may be the cause of CAP failure. Accumulating $[K^+]_o$ can act to depolarise the axonal membrane, preventing the recovery of Na^+ channel inactivation (Hodgkin and Huxley, 1952b), which in turn, reduces the number of Na^+ channels available for Na^+ to move through. Consequently, both the rate of membrane depolarisation and CAP amplitude is decreased, as determined by ENa, as we have previously discussed. Therefore, we must investigate whether $[K^+]$ accumulates in the extracellular space sufficiently during high frequency stimulation to induce a fall in CAP amplitude. The MON was stimulated at a high frequency, as K^+ sensitive microelectrodes measured the $[K^+]_o$. It can be seen in figure 21, that during the imposition of a 2-minute stimulation at 100 Hz, the $[K^+]_o$ response had a distinctive profile with four focal parameters- (1) the rate of $[K^+]_o$ rise; (2) an overshoot; (3) the plateau phase; (4) an undershoot. The first to note is the steep rate of rise upon stimulation, where the $[K^+]_o$ increases. Next an overshoot can be observed by $[K^+]_o$, up to ~4.3 mM from its physiological baseline of 3 mM. This overshoot then gradually declines down to ~3.8 mM during stimulation where $[K^+]_o$ begins to plateau, considered as the second baseline. Upon cessation of stimulation, $[K^+]_o$ falls back down at a slower rate, where an undershoot below the physiological concentration of 3 mM, to ~2.2 mM is observed. Finally, $[K^+]_o$ gradually relaxes back towards its original baseline concentration (3 mM).

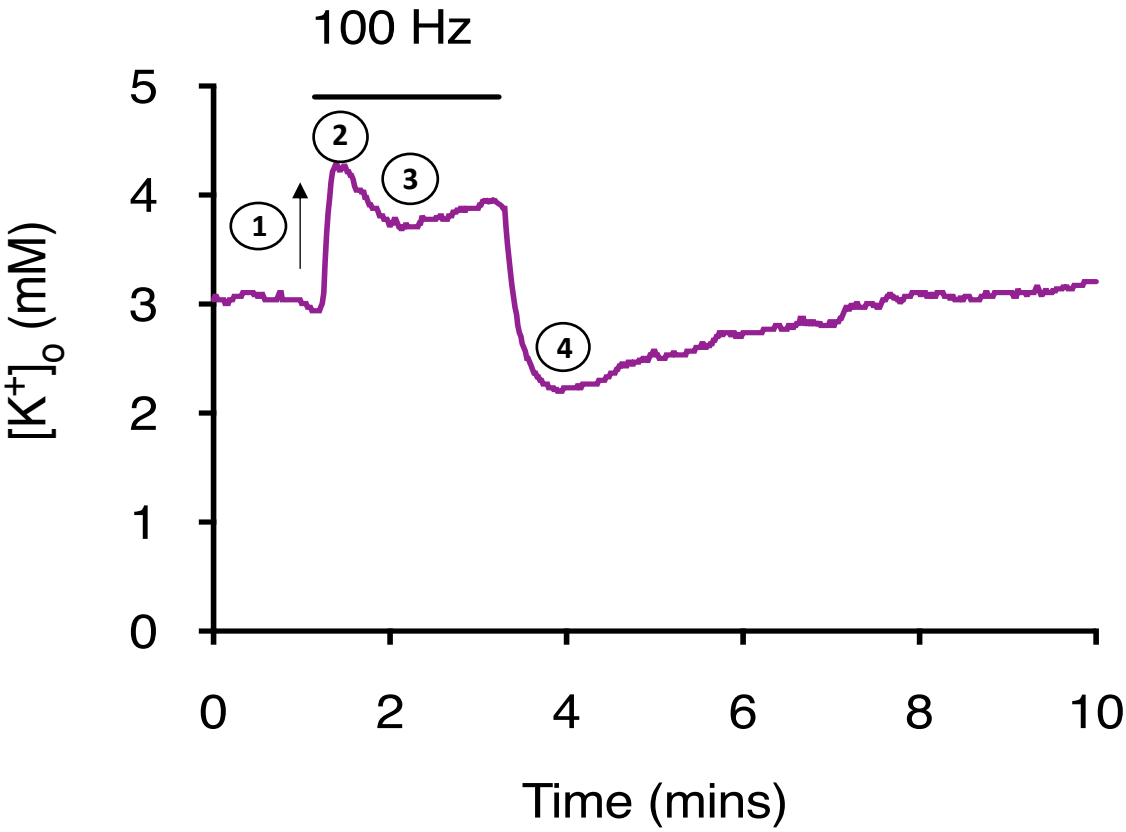

Figure 21: The effects of a high frequency stimulation on $[K^+]_o$.

The MON was stimulated at 100 Hz for 2 minutes (as indicated by the bar above the stimulation) as K^+-sensitive microelectrodes measured $[K^+]_o$. (1) During stimulation $[K^+]_o$ sharply increases. (2) It then overshoots from the physiological concentration of 3 mM up to ~4.4 mM. (3) This is followed by a decrease down to a secondary plateau phase at ~3.8 mM. (4) $[K^+]_o$ then gradually falls again during the cessation of the stimulus, undershooting below its original baseline of 3 mM to ~2.2 mM. A gradual relaxation back to its original baseline concentration (3 mM) can then be observed.

Considerable research has been previously conducted investigating $[K^+]_o$ within the optic nerve (Ransom et al., 2000) (Connors et al., 1982) (Bay and Butt, 2012), however we are only interested in a few specific aspects. This includes the maximal concentration reached by extracellular K^+ during stimulation and the profile of this increase compared to the falling CAP amplitude. It can be observed in figure 21, that the $[K^+]_o$ response has four focal parameters when stimulated, the first of which is an increase in $[K^+]_o$. It can be seen in figure 22, that as the stimulus frequency was progressively increased from the physiological frequency of 5 Hz, up to 10, 20, 33, 50, 67, 80, 100 and 200 Hz, $[K^+]_o$ logarithmically increased in a frequency dependent manner . At 10 Hz, $[K^+]_o$ reached 3.2 mM, showing a minimal increase from its baseline concentration. However, during a 200 Hz stimulation, $[K^+]_o$ was elevated up to 4.0 mM. This maximal concentration during a high frequency stimulation is consistent with our findings in figure 21, where $[K^+]_o$ reached ~4.4 mM during a 100 Hz stimulation for 2 minutes.

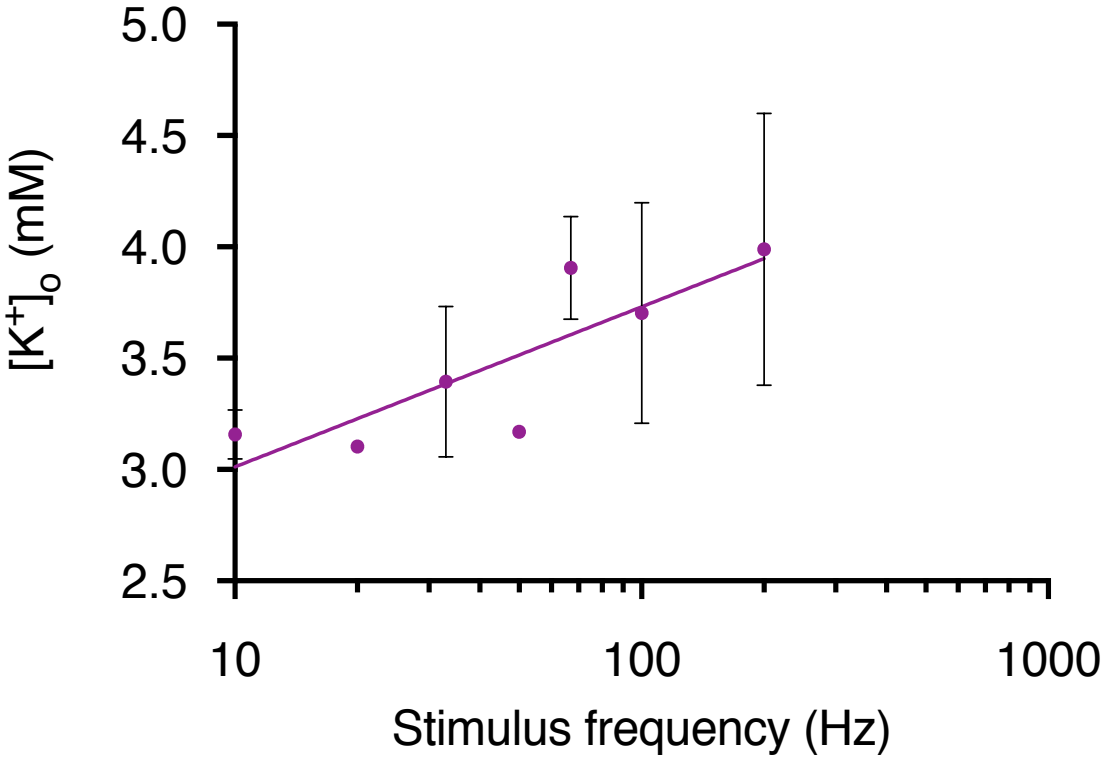

Figure 22: $[K^+]_o$ logarithmically increases with stimulus frequency.

As stimulus frequency was progressively increased from the physiological frequency of 5 Hz, up to 10, 20, 33, 50, 67, 100 and 200 Hz, $[K^+]_o$ (mM) increased logarithmically from its baseline concentration of 3 mM. During a 200 Hz stimulation $[K^+]_o$ reached 4.0 mM (SD = 0.6) (n = 4), consistent with that found in figure 21 during a 2 minutes stimulation at 100 Hz. (SD is represented by the vertical bars seen above and below each data point).

The undershoot observed in $[K^+]_o$ upon the cessation of stimulation was not initially an area we had intended to investigate, however as experiments progressed it became an exigent parameter which became difficult to ignore. It can be observed in figure 23, that there was a period of undershoot in $[K^+]_o$ from its baseline concentration of 3 mM upon the cessation of stimulation, which increased in magnitude as the frequency of the stimulus train increased (20, 33, 50, 67, 100 or 200 Hz). This effect was observed to be most pronounced following the highest stimulus frequencies, with a 200 Hz stimulation inducing $[K^+]_o$ to decrease beyond its baseline concentration to 2.7 mM.

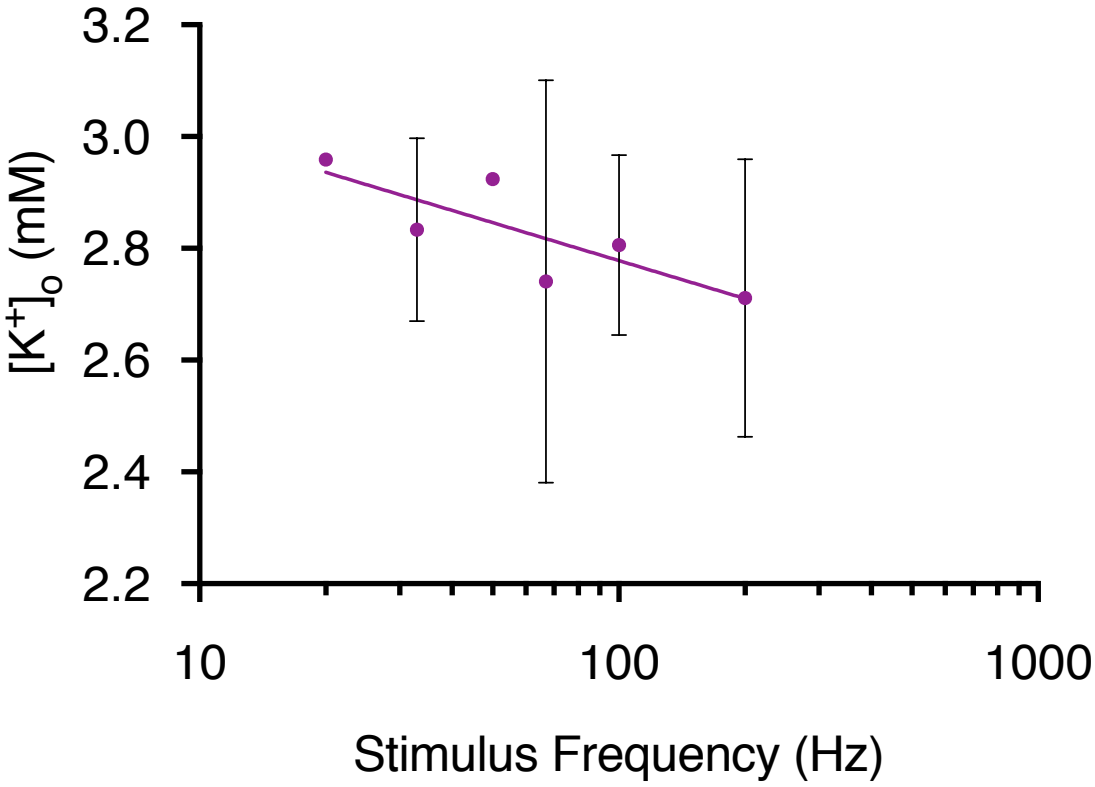

Figure 23: $[K^+]_o$ undershoot upon the cessation of varying stimulus frequencies.

$[K^+]_o$ (mM) is plotted against the frequency of a preceding stimulation (Hz) on a $\log_{10}$ scale. $[K^+]_o$ undershoots its baseline concentration (3 mM) upon the cessation of stimulation, the extent to which is dependent upon the stimulation frequency preceding it (20, 33, 50, 67, 100 or 200 Hz). The greatest undershoot is observed following a 200 Hz stimulation where $[K^+]_o$ fell from ~3 mM, down to 2.7 mM (SD= 0.3) (n = 4). (SD are represented by the vertical bars shown above and below each data point).

The recovery from this $[K^+]_o$ undershoot back to the baseline concentration of 3 mM was also observed to vary in duration, depending upon the stimulation frequency preceding it. It can be observed that as the stimulus frequency increased from the physiological frequency of 5 Hz, up to 10, 33, 50, 67, 100 and 200 Hz, the duration required for $[K^+]_o$ to return back to baseline increased (figure 24). Following a 10 Hz stimulation, it took 0.9 minutes for $[K^+]_o$ to return to 3 mM. However, after a stimulation at 200 Hz, this took 2.5 minutes. When fit with a linear regression, it can be seen that the time for $[K^+]_o$ recovery occurred in a manner determined by the preceding frequency stimulation.

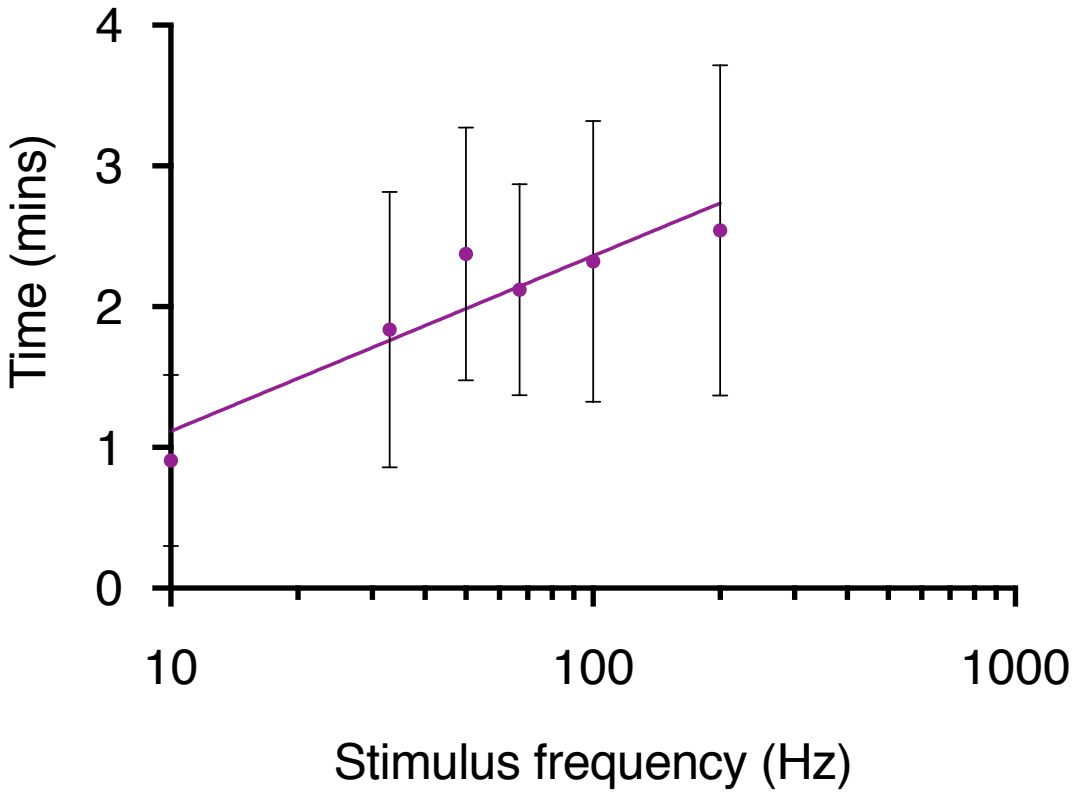

Figure 24: The duration for $[K^+]_o$ recovery following varying frequency stimulations.

The duration required for $[K^+]_o$(mM) to recover back to a 3 mM baseline was plotted against the frequency of a preceding stimulation (Hz) on a $\log_{10}$ scale and fit with a linear regression. The duration for $[K^+]_o$ to recover to baseline progressively increased with the stimulation frequency preceding it (10, 33, 50, 67, 100 or 200 Hz). Following a 10 Hz stimulation, $[K^+]_o$ took 0.9 mins (SD = 0.6) (n = 5) to relax back to baseline, compared 2.5 mins (SD = 1.2) following a 200 Hz stimulation (n = 4). (SD are represented by the vertical bars shown above and below each data point).

It is appreciated that $[K^+]_o$ accumulates in an activity dependent manner within the extracellular space and can reach an appreciable concentration (Ransom et al., 2000), which could cause the CAP amplitude to fall (Hodgkin and Huxley, 1952a). Therefore, the CAP was recorded as $[K^+]$ was incrementally increased in the aCSF, in order to investigate the effects on CAP amplitude. It can be observed from figure 23, that as $[K^+]_o$ is increased from the physiological concentration of 3 mM up to 9, 10.5, 12, 13.5, 15 and 18 mM, the CAP amplitude progressively falls during a supramaximal stimulation, seen in a uniform manner across all three peaks of the CAP. This is due to K^+ in the aCSF increasing throughout the entire extracellular fluid which therefore has a generalised effect on all axons equally. As a result, the second peak of the CAP was selected for illustrative purposes (figure 23). This effect was observed to be the most pronounced when stimulated during the highest extracellular K^+ concentrations tested (15 and 18 mM). At these concentrations, the CAP can be observed to completely fail (figure 23).

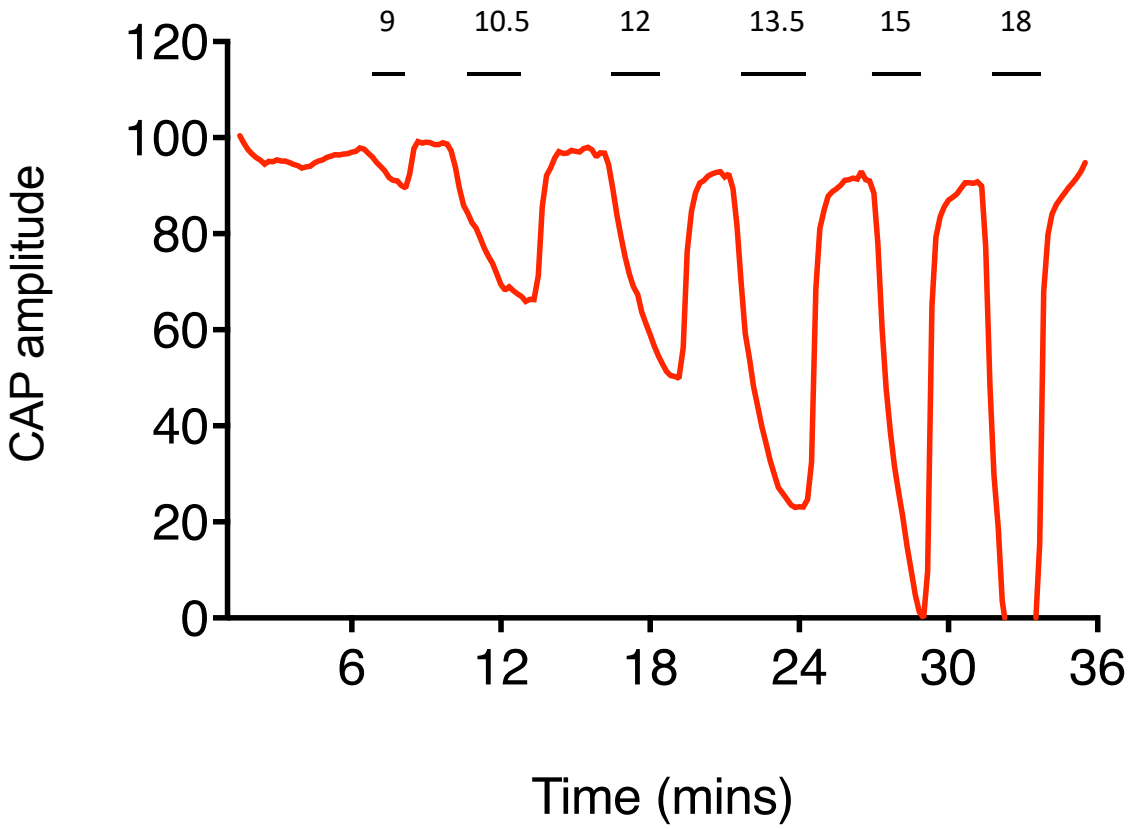

Figure 25: The effects of increasing $[K^+]_o$ on second peak CAP amplitude.

The $[K^+]_o$ within the aCSF bathing the MONs was incrementally increased from the physiological baseline of 3 mM, up to 9, 10.5, 12, 13.5, 15 and 18 mM (as indicated by the bars above each supramaximal stimulation). CAP amplitude progressively fell with increasing $[K^+]_o$ in a concentration dependent manner, resulting in complete conduction failure at 15 and 18 mM.

It has previously been shown by Hodgkin and Huxley (1952a), that as $[K^+]_o$ is progressively increased, the onset of CAP failure during a supramaximal stimulation does not occur until $[K^+]_o$ reaches >9mM. This is consistent with our results as seen in figure 24, where the $[K^+]_o$ was incrementally increased from the physiological concentration of 3 mM up to 9, 10.5, 12, 13, 15 and 18 mM and plotted against CAP amplitude. When fit with a linear regression, it can be observed that between 3 and 9 mM $[K^+]_o$, the CAP amplitude remains constant, normalised to 100. However, as $[K^+]_o$ is increased beyond 9 mM, the CAP begins to rapidly fall in amplitude. This suggests that our results in section 3.4, are not influenced by $[K^+]_o$ reducing the number of available Na^+ channels for Na^+ to move through as a $[K^+]_o$ concentration of >9 mM is unlikely to be achieved due to the extensive propensity of astrocytes to buffer $[K^+]_o$.

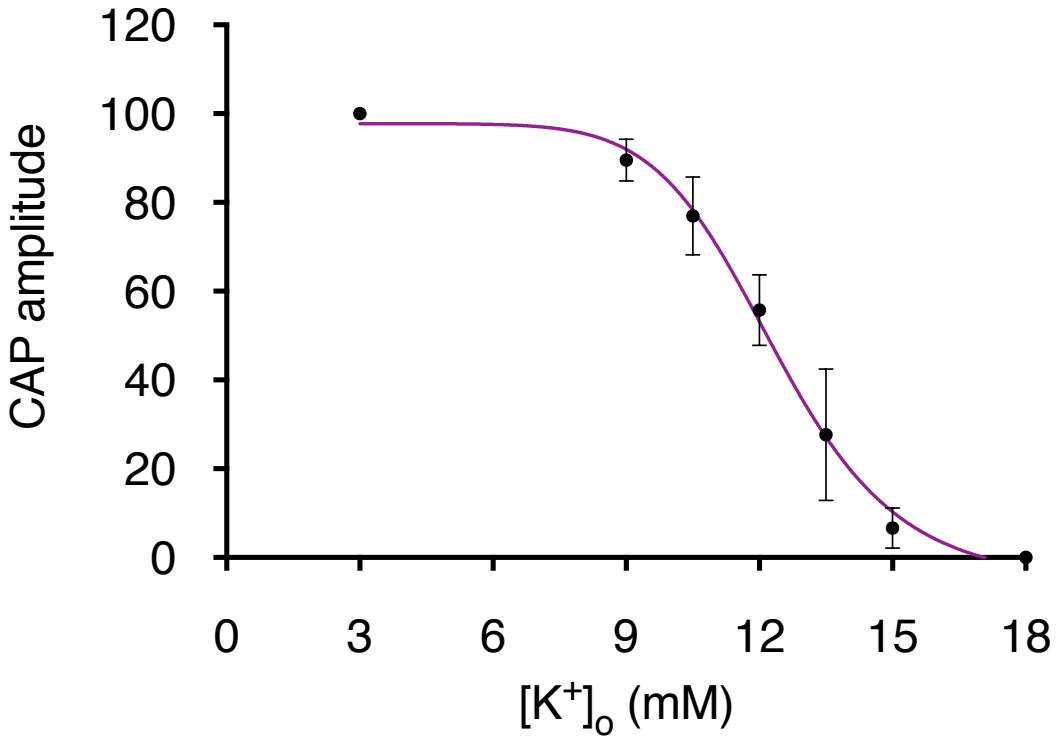

Figure 26: The effects of increasing $[K^+]_o$ on CAP amplitude.

Increasing $[K^+]_o$ from its baseline concentration of 3 mM, up to 9, 10.5, 12, 13, 15 and 18 mM was plotted against the normalised CAP amplitude and fit with a linear regression. The CAP amplitude remained constant with increasing up $[K^+]_o$ until 9 mM. Once 9 mM is surpassed, a progressive fall towards 0 mV can be seen in CAP amplitude, in a concentration dependent manner (EC_{50} = 12.3 mM, slope = 9.7). CAP failure occurs at 18 mM $[K^+]_o$, as the amplitude reaches 0 mV. (SD is indicated by the vertical bars above and below each data point).

We then wanted to investigate the profile of the $[K^+]_o$ response during stimulation, compared to the profile of the falling CAP amplitude. Therefore we recorded both $[K^+]_o$ and the CAP simultaneously, which to the best of our knowledge is the first time this has been done. The effects of a high frequency stimulation (100 Hz) for 2 minutes on $[K^+]_o$ and CAP amplitude were demonstrated by superimposing the two respective traces. It can be observed from figure 25, that during this stimulation, $[K^+]_o$ rapidly increases from the physiological concentration of 3 mM, up to ~4.4 mM, as we previously observed in figure 19. Meanwhile, the CAP amplitude of the second peak falls, as we would expect. However, when the traces are overlapped, it can be observed that the rate of rise of $[K^+]_o$ and fall of CAP amplitude during stimulation do not mirror each other- $[K^+]_o$ rises at a much faster rate than the fall seen in CAP amplitude. Upon cessation of the 100 Hz stimulus, $[K^+]_o$ undershoots, before gradually returning to its baseline concentration of 3 mM, as the CAP amplitude overshoots before gradually returning to its normalised baseline. However, unlike at the start of stimulation, during cessation, the rate of recovery for $[K^+]_o$ and CAP amplitude do appear to mirror each other. This therefore suggests that during a high frequency stimulation, $[K^+]_o$ does not dictate the fall in CAP amplitude, however may affect its recovery post-stimulus.

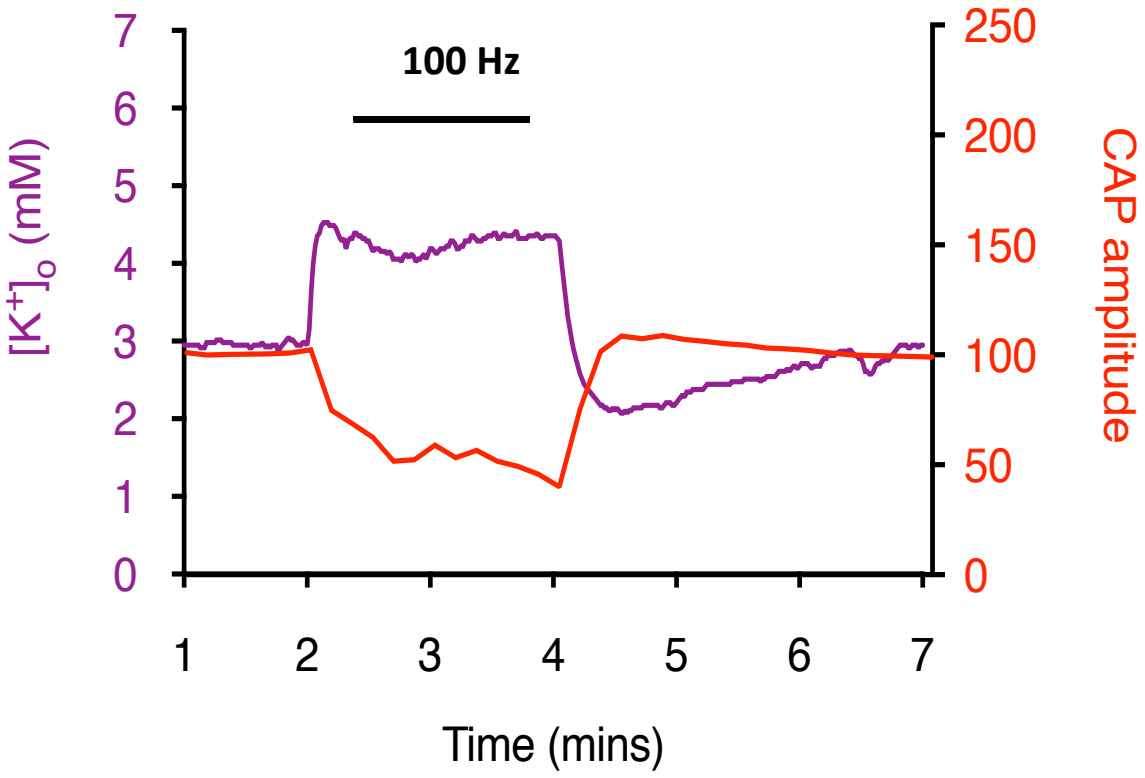

Figure 27: Superimposed traces of $[K^+]_o$ and CAP amplitude during a high frequency stimulus.

The effects of a 100 Hz stimulation for 2 minutes (as represented as the bar above the stimulation) on $[K^+]_o$ (mM) and CAP amplitude (mV) are superimposed onto the same graph. At the onset of stimulation, there is a rapid increase in $[K^+]_o$ (purple trace) up towards 4.4 mM from the physiological concentration of 3 mM. During the same stimulation, the CAP amplitude (red trace) is observed to decrease, however at a more gradual rate. The rate of rise of $[K^+]_o$ and fall of CAP amplitude do not appear to mirror each other. Upon cessation of the 100 Hz stimulation, $[K^+]_o$ undershoots before gradually returning towards its original baseline concentration (3 mM). CAP amplitude overshoots its original baseline before gradually returning to its normalised baseline amplitude. The rate of recovery for $[K^+]_o$ and CAP amplitude can be observed to mirror each other, suggesting $[K^+]_o$ may dictate CAP amplitude recovery post stimulation.

The effect of $[K^+]_o$ on the recovery of the CAP amplitude post-stimulus can be seen in greater detail in figure 28. The $[K^+]_o$ in the aCSF bathing the nerves was decreased from its baseline concentration of 3 mM, down to 2.5 and 2 mM and then followed by a 100 Hz stimulation. It can be observed that as $[K^+]_o$ is decreased, the CAP amplitude increases due to a hyperpolarisation of the reversal potential for K^+. This in turn, releases the inactivation of some Na^+ channels, priming them to fire upon the next stimulation. During the stimulation, the CAP amplitude decreases as we would expect, however this is followed by an overshoot beyond its baseline amplitude upon the cessation of this stimulus. As all three of the CAP peaks were affected to the same extent during stimulation, it is predicted that the reductions in $[K^+]_o$ dictate the amplitude of the CAP overshoot.

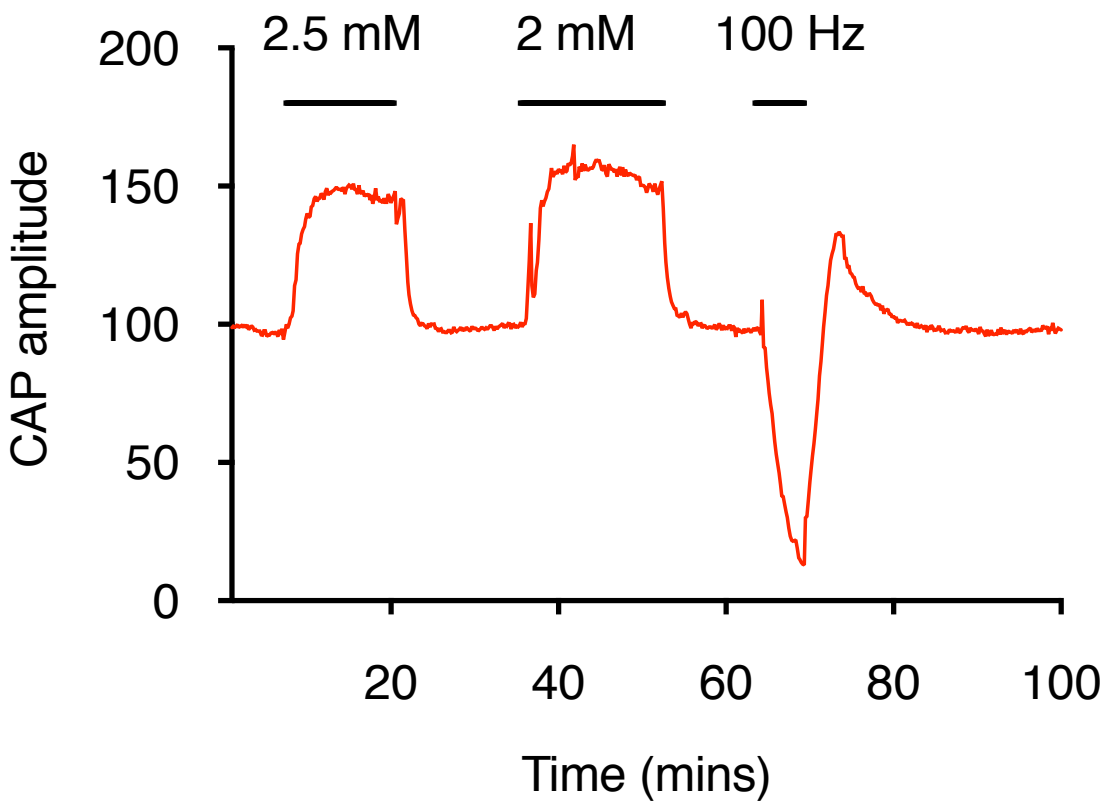

Figure 28: The effects of decreasing $[K^+]_o$ followed by a high frequency stimulation on the CAP overshoot.

$[K^+]_o$ was reduced in the aCSF bathing the nerves from its baseline concentration of 3 mM, down to 2.5 and 2 mM, followed by a 100 Hz stimulation (as represented by the bars above). As $[K^+]_o$ was decreased, the CAP amplitude progressively increased in amplitude. When followed by a 100 Hz stimulation, the CAP amplitude fell, which then recovered during the cessation of stimulation where it overshot its normalised baseline amplitude.

Figure 29 illustrates a summary of our findings from the previous data. The top blue bar represents $[K^+]_o$ during a 100 Hz stimulation to the MON for 5 minutes. It can be seen that $[K^+]_o$ only increases to ~4 mM, as we have seen in figures 21 and 22, however undershoots its baseline concentration of 3 mM upon the cessation of the stimulus (as observed in figures 21 and 23). Below, the three peaks of the CAP are illustrated, falling in a differential manner during the stimulation. The first peak of the CAP (red trace) remains the most robust during stimulation, decreasing the least in amplitude. The second peak (blue trace) falls to an intermediate degree and the third peak (orange trace) can be seen to be the most sensitive to this stimulation, falling the most in amplitude out of the three peaks (as seen in figure 14, 15 and 16). Following cessation of the stimulus, all three peaks can be observed to overshoot their baseline amplitude to the same extent, before gradually recovering (as seen in figure 27). Respective traces of the CAP profile during this stimulation are shown below in pink. Finally, the concentration of $[Na^+]_i$ during stimulation is demonstrated, accumulating the least in the first peak of the CAP (~20 mM), followed by the second peak (~40 mM) and then the third peak, where $[Na^+]_i$ accumulated the most (~60 mM).

3.6 A summary of the effects of high frequency stimulation on $[K^+]_o$, CAP amplitude, CAP profile and $[Na^+]_i$.

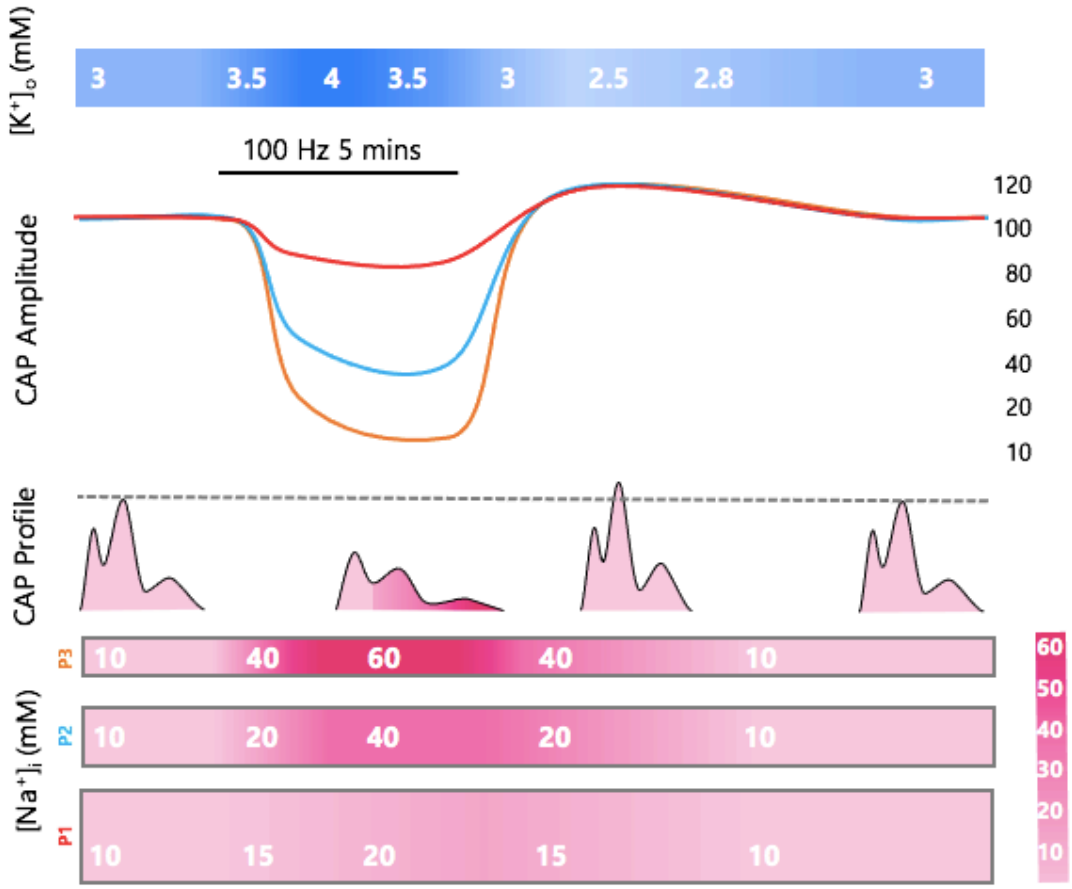

Figure 29: A summary of the effects of high frequency stimulation on $[K^+]_o$, CAP amplitude, CAP profile and $[Na^+]_i$.

The effects of a 100 Hz stimulus for 5 minutes to the MON is illustrated. $[K^+]_o$ can be seen to accumulate to ~4mM during stimulation. Upon the cessation of the stimulus, $[K^+]_o$ gradually decreases and undershoots its baseline concentration of 3 mM, before slowly recovering. The differential effects on the three peaks of the CAP amplitude are seen next, with the first peak remaining the most robust during stimulation (red trace), followed by the second peak (blue trace) and then the third peak (orange trace) which decreased the most in amplitude. Upon cessation of the stimulus, all three peaks of the CAP are seen to overshoot to the same extent, before gradually returning to their baseline amplitude. Respective traces of the CAP profile during this stimulation are shown below in pink. Finally, the accumulation of $[Na^+]_i$ is shown in the three peaks of the CAP, shown to accumulate the most in the third peak (60 mM) and least in the first peak (20 mM).

Chapter 4: Discussion

Our results provide further support for the existence of three distinct sub-populations of axon diameter, which generate the triphasic CAP profile, as originally proposed by Allen et al (2006). It is suggested that axons with the largest diameters contribute to the first peak of the CAP, while those intermediate and smallest in diameter contribute to the second and third CAP peaks, respectively. These three sub-populations defined by axon diameter bestow differential bio-physical properties due to their surface area-to-volume ratio considerations, which govern their ability to withstand high frequency firing. Therefore, during high frequency stimulation, the three CAP peaks fall in a differential manner, which we have quantified through extracellular electrophysiological recordings and subsequent analysis. We have also challenged the original dogma that this fall in CAP amplitude during high frequency stimulation is as a result of elevated $[K^+]_o$, as we provide evidence through indirect methodology to alternatively support a $[Na^+]_i$ accumulation hypothesis. Our conclusions in this regard are based upon the following observations: (1) during incremental increases in the stimulus voltage, the first peak of the CAP was recruited at the lowest stimulus intensity, followed by the second and third peaks, respectively; (2) as stimulus frequency was progressively increased beyond 5 Hz, there was a frequency dependent fall in the CAP across all peaks of the CAP, however most pronounced in the third peak, considered to be contributed to by axons with the smallest diameter; (3) the CAP amplitude did not begin to fall until >9 mM $[K^+]_o$, which is unlikely to be reached as a result of physiological stimulus due to the astrocytic capacity to spatially buffer $[K^+]_o$; (4) during high frequency stimulation, $[Na^+]_i$ was calculated to accumulate the most in the third peak of the CAP, followed by the second and first peaks, respectively.

4.1 Evidence for the existence of three distinct sub-populations of axon diameter.

Our first experimental procedures provide evidence for the existence of three distinct sub-populations of axon diameter, which underpin the triphasic profile of the MON CAP. We used the MON as a model of central white matter due to its accessibility and lack of complications due to its composition of only myelinated axons and glia (Evans et al., 2010). It also ensured that our experimental procedures were in accordance with the NC3Rs, as each mouse provided an n of 2 nerves which were utilised for independent recordings (Rich et al., 2020). This model has been utilised extensively in previous research and ensures compatibility with future transgenic and spontaneous mutant models. However, CD-1 mice are albino and may suffer from impaired vision which we cannot be certain does not affect their visual processing (Adams et al., 2002). We therefore also investigated the effects of high frequency stimulation on a different strain of mouse- C57BL/6, where minimal differences were observed. Therefore, CD-1 mice appeared to be an appropriate strain to use for our experimental procedure.

Our results have demonstrated how incrementally increasing the stimulus voltage recruits the three peaks of the CAP in a sequential manner, beginning with the first peak which exhibited the lowest threshold for activation (figure 8). The second peak was observed to be recruited next at an intermediate stimulus voltage, followed by the third peak which demonstrated the highest threshold for activation (figure 8). Due to all of the axons within the MON being myelinated, it is assumed that the differences observed in threshold activation are likely due to axon diameter. These findings were further reinforced when the area of each peak was converted to a cumulative probability function, demonstrating the cumulative distribution of the three peaks during increasing stimulus voltage (figure 9). It could be seen again that the first peak of the CAP was recruited at the lowest stimulus intensity, followed by the second and third peaks, respectively. These results are as we would expect if the triphasic profile of the CAP was reflected by the heterogeneous velocity of propagation of various axons. This is due to the relationship between axon diameter and axoplasmic

resistance being quadratic in nature, compared to membrane resistance which varies linearly (Allen et al., 2006). Therefore, a doubling in axon diameter would decrease the axoplasmic resistance to a greater extent than the membrane resistance, resulting in less stimulus voltage required for recruitment compared to smaller diameter axons, as current flow favours travel down the path of least resistance.

When values for the mean ± SD obtained by fitting the data in figure 9 with a cumulative probability function were used to generate Gaussian distributions for each of the CAP peaks (figure 10), the subsequent distribution was almost identical to the CAP profile (figure 11), providing further evidence for the existence of three sub-populations of axon diameter. However, a superimposition can be observed between the first and second peaks, which suggests that rather than there being three discrete axon diameters, there exists a wide distribution which are categorised into their most suitable sub-population, based upon their conductance properties. Our double pulse protocol implemented in figure 13 further supports this theory, as a low stimulus voltage only recruited the first peak of the CAP, however when followed immediately by a second higher intensity stimulus, only the second and third peaks were recruited (figure 13). This suggests that all axons contributing to the first peak remained inactivated during the second stimulation and therefore, each axon only contributes to one individual peak.

Our findings were consistent with those found previously by Allen et al (2006) who first proposed this hypothesis, which together provides convincing evidence for a heterogenous population of axons, categorised into three distinct sub-populations based upon diameter.

4.1.2 Larger diameter axons within the MON facilitate higher information transfer rates and neuronal firing.

The existence of a wide distribution of axon diameters within the MON (Perge et al., 2009) challenges the original dogma which suggests that larger axons predominate in longer CNS tracts requiring faster conduction. While the conduction time hypothesis is valid in this context, it does not explain the presence of larger diameter axons within the optic nerve- a short CNS tract with a conductance distance to the lateral geniculate nucleus of only 17mm, as shown in the guinea pig (Perge et al., 2009). An increase in axon diameter would therefore only increase information arrival time by a fraction, which due to space and energy and space constraints would not justify their presence. However, we have proposed an alternative advantage for larger diameter axons within the optic nerve and hypothesise that their existence would facilitate higher information transfer rates and neuronal firing frequency. Our stimulus frequency experiments show that as the stimulus frequency was increased from the physiological frequency of 5 Hz, up to 100 Hz, the three peaks of the CAP fall in a frequency dependent manner, however to different extents (figures 14, 15 and 16). The first peak of the CAP, thought to be contributed to by the largest diameter axons, was consistently more capable of maintaining its amplitude during supraphysiological stimulations. The amplitude did not fall until stimulation reached 40 Hz and upon increasing this stimulation to 100 Hz, only a ~17% fall was observed from its normalised baseline (figure 15). The second peak remained intermediate in sensitivity out of the three peaks during stimulation (~63% fall), while the third peak exhibited the most drastic effects, falling by ~88% in amplitude from its normalised baseline at 100 Hz (figure 15). These findings suggest that larger diameter axons are endowed with a greater capacity to withstand high frequency firing, compared to those with a smaller diameter, thought to be as a result of a greater metabolic supply. It must be realised that as an axon doubles in diameter, its surface area would increase linearly, compared to its axonal volume, which would increase as a squared function (Perge et al., 2009). Therefore, there would be a quadratic increase in the

internal mitochondrial volume fraction for a 2-fold increase in the membranous ion channels, permitting a much greater ATP supply to fuel activity dependent Na^+/K^+/ATPase pumps. These pumps are responsible for re-equilibrating transmembrane ion gradients after the firing of an action potential (Pirahanchi and Aeddula, 2019). Once the transmembrane gradients are reset, the K^+ conductance is very high and contributes to the after hyperpolarisation of an axon, which cannot be overcome by current input (Zhang and McBain, 1995). Therefore, the refractory period must conclude before the next impulse can occur. Although energy constraints imposed by physiological challenges such as high frequency firing can be met via functional hyperaemia within physiological limits, exceptionally high stimulus frequencies overwhelm the system and functional hyperaemia is no longer sufficient to sustain neuronal firing. Therefore, under these conditions, smaller diameter axons have insufficient ATP to fuel the Na^+/K^+/ATPase pumps and the transmembrane ion gradients cannot be adequately re-distributed after an electrical impulse. This decreases the concentration gradient across the plasma membrane and causes ENa to fall towards 0mV, reducing the driving force for Na^+ influx. As a result, the CAP amplitude progressively decreases with each succeeding stimulation as Na^+ influx is responsible for the peak of the action potential. This is exactly as we observed in our results during increasing frequency stimulation (figures 14, 15 and 16).

4.2 Evidence disputing $[K^+]_o$ as the driving force for CAP fall during high frequency firing.

It was originally proposed that this fall in CAP amplitude during high frequency stimulation was due to a build-up of K^+ within the extracellular space. It is a universal property of excitable tissue to liberate K^+ from the axon into the extracellular space during neuronal activity, as the action potential repolarises. This liberation is linear and proportional to the stimulus frequency (Hodgkin and Huxley, 1953) and can accumulate to a significant extent. Therefore, we

investigated the effects of accumulating $[K^+]_o$ during high frequency stimulation on the CAP amplitude using K^+-sensitive microelectrodes.

We first checked that the time interval between stimulations was sufficient for the refractory period to have concluded and that a loss of CAP amplitude was not as a result of Na^+ channel inactivation. This was investigated by implementing a double pulse protocol, where the time interval between the two stimulations was gradually decreased. It could be seen from figure 12, that decreasing the stimulation interval down to 5 ms (equivalent to 200 Hz) has a negligible effect on the CAP amplitude across all three peaks and we could therefore rule out the time interval between stimulations as a cause of decreasing CAP amplitude in any future experiments.

In order to investigate the effects of high $[K^+]_o$ on the CAP amplitude, $[K^+]_o$ was incrementally increased in the aCSF bathing the nerves. It can be observed that the CAP amplitude remained constant until $[K^+]_o$ exceeded 9 mM. (figure 26). However, further increases beyond 9 mM induced a progressive fall in CAP amplitude, with complete conduction failure occurring between 15-18 mM (figures 25 and 26). This effect was uniform across all three peaks of the CAP which is thought to be due to $[K^+]$ within the aCSF increasing throughout the entire extracellular fluid and therefore having a generalised effect on all axons equally. It has been proposed that this fall in CAP amplitude during elevated $[K^+]_o$ (> 9 mM) occurs due to positively charged $[K^+]_o$ within close proximity to the axonal membrane acting to depolarise it, preventing the recovery of Na^+ channel inactivation (Hodgkin and Huxley, 1952b). This in turn, reduces the number of Na^+ channels available for Na^+ to move through and thus, the rate of membrane depolarisation, in addition to the CAP amplitude, as determined by ENa. This would explain our results observed in figures 25 and 26.

When investigating the effects of high frequency firing on $[K^+]_o$ accumulation, recorded using K^+- sensitive microelectrodes, it can be seen that $[K^+]_o$ increased in a linear and proportional manner with stimulus frequency (figure 22). This is as we would expect as each individual action potential liberates a consistent concentration of K^+ from the axon into the extracellular space (Frankenhauser and Hodgkin, 1956). Therefore, as the stimulus frequency is increased, so too is

the number of axons firing and thus, $[K^+]_o$ efflux. However this highly supraphysiological stimulation (2 minutes at 100 Hz) only caused $[K^+]_o$ to accumulate to ~4 mM from a baseline of 3 mM (figures 21 and 22). It is therefore unlikely for accumulating $[K^+]_o$ to be the cause of the CAP failure observed during high frequency stimulation (figures 14, 15 and 16), as this concentration is insufficient to prevent the recovery of Na^+ channel inactivation. This ceiling value is considered to be a result of the propensity for local astrocytes to spatially buffer $[K^+]_o$. Astrocyte spatial buffering relies upon the membrane potential of astrocytes localised to areas of high neuronal activity being negative relative to the reversal potential of K^+, providing a driving force for the uptake of K^+ out of the extracellular space and into the astrocytes (Orkand et al., 1966). This mechanism of $[K^+]_o$ clearance is extremely effective and provides an explanation for a ceiling $[K^+]_o$ level during high frequency firing. These results are consistent with previous findings by Connors et al (1982), who also found that $[K^+]_o$ evoked in mature rat optic nerves during a supramaximal stimulus had a ceiling level (~9.8 mM). Although this is a higher concentration than what we found, it still appears improbable when reviewing figure 26 to be the cause of the CAP amplitude fall that we observed during high frequency stimulation. It is important to note that we used adult CD-1 mice for all experiments as evidence suggests that the ceiling level of $[K^+]_o$ evoked during supramaximal stimulation is maturation dependent, due to changes in activity dependent K^+ accumulation with postnatal age and tissue maturity (Connors et al., 1982). This is thought to be as a result of astrocytic immaturity in younger rodents, which has been demonstrated by administration of the mitotic inhibitor 5-azacytidine (5-AZ) to neonatal rat optic nerves, which is known to disrupt gliogenesis. It was observed that upon administration to the optic nerve, there was a significantly higher activity dependent accumulation of $[K^+]_o$, as compared to control animals (Yamate and Ransom, 1985). This demonstrates the importance of using mature animal models for experimental investigations. Further evidence that a fall in CAP amplitude during high frequency stimulation is not due to $[K^+]_o$ elevations comes from our novel simultaneous recordings of the CAP and $[K^+]_o$ responses. It can be seen in figure 27, that as $[K^+]_o$ rises during a

100 Hz stimulation, the CAP amplitude decreases. However, the rate of $[K^+]_o$ rise and CAP fall do not mirror each other- $[K^+]_o$ is observed to rapidly increase, whereas the fall in CAP amplitude is more gradual. It is therefore suggested that accumulating $[K^+]_o$ does not dictate the CAP response and another variable must be influencing the fall in CAP amplitude.

4.3 $[Na^+]_i$ accumulation during high frequency firing.

We hypothesised that the fall in CAP amplitude during high frequency firing was not as a result of accumulating $[K^+]_o$ but alternatively accumulating $[Na^+]_i$. Our $[K^+]_o$ evidence suggested that K^+ was unlikely to reach sufficient concentrations in the extracellular solution to induce CAP failure. Therefore, we investigated the effects of accumulating $[Na^+]_i$ on CAP amplitude which has frequently been overshadowed by the widely accepted $[K^+]_o$ dogma. This may largely be due to the seminal work of Frankenhauser and Hodgkin (1956), who conducted their investigations in the *Loligo* squid, which possesses an external barrier to confine $[K^+]_o$ close to the axolemma, therefore preventing its diffusion away and exacerbating membrane depolarisation. Additionally, it proves impossible to achieve accurate real-time measurements of $[Na^+]_i$ directly in the nodes of myelinated axons of different sizes, limiting the potential for $[Na^+]_i$ to be investigated.

Our logic behind our $[Na^+]_i$ hypothesis is such that accumulating $[Na^+]_i$ would act to reduce the transmembrane concentration gradient of Na^+ across the plasma membrane. This would in turn, reduce the driving force for Na^+ influx since extracellular $[Na^+]$ would remain unchanged, reducing the ratio of $[Na^+]_o$: $[Na^+]_i$ and thus, causing ENa to fall towards 0mV. As Na^+ influx is responsible for the peak of the action potential, we would expect the amplitude to decrease, as reflected by a reduction in CAP amplitude.

To investigate this, we devised an indirect methodology permitting estimations of $[Na^+]_i$ through reductions in $[Na^+]_o$, followed by manipulation of the Nernst equation, as inspired by Hodgkin and Huxley (1952a) during their work to

quantify the leak current. It can be seen in figure 17, that as $[Na^+]_o$ in the aCSF was decreased, the CAP progressively fell in amplitude in a concentration dependent manner and increased in latency. This is as we predicted, as a reduction in $[Na^+]_o$ would act to mimic the effects of accumulating $[Na^+]_i$ by reducing the Na^+ concentration gradient across the plasma membrane and therefore ENa. This effect was uniform across all three peaks of the CAP, thought to be due to the same $[Na^+]$ bathing the axons within the MON, which therefore had a generalised effect on ENa across all axons. Therefore, the second peak was selected for illustration (figure 17). When plotted on a logarithmic scale, an explicit equation between $[Na^+]_o$ and CAP amplitude could be derived (figure 18) and used to solve for estimations of ENa and $[Na^+]_i$, as $[Na^+]_o$ remained unchanged during high frequency stimulus. These calculated values for ENa and $[Na^+]_i$ were then plotted against stimulus voltage (figure 19), where ENa can be observed to decrease with increasing frequency, as $[Na^+]_i$ increases. The way in which ENa and $[Na^+]_i$ mirror each other reflects how $[Na^+]_i$ directly influences the value of ENa.

4.3.1 The differential sensitivity of axon sub-populations to accumulating $[Na^+]_i$

We then set out to investigate whether the extent of $[Na^+]_i$ accumulation was influenced by axon morphology. Therefore, calculated values for $[Na^+]_i$ were then plotted against stimulus frequency on a logarithmic scale for each of the three peaks of the CAP (figure 20). It could be observed that as stimulus frequency increased from the physiological frequency of 5 Hz, up to 100 Hz, $[Na^+]_i$ accumulated in all three peaks in a frequency dependent manner, however to different extents. The first peak was observed to accumulate $[Na^+]_i$ the least, reaching 22.3 mM (SD= 13.0) at 100 Hz stimulation, followed by the second peak (44.7 mM (SD= 10.3). However, the third peak of the CAP accumulated $[Na^+]_i$ to the greatest extent, reaching 62.9 mM (SD= 9.5) during a 100 Hz stimulation. This differential manner in which the three peaks of the CAP accumulated $[Na^+]_i$ is thought to be an indirect result of the morphology of the axons contributing to

each peak. We have proposed that the largest diameter axons contribute to the first peak of the CAP and due to surface area-to-volume ratio considerations, have a much greater mitochondrial volume fraction, as compared to the number of membranous Na^+/K^+/ATPase pumps. Therefore, they have a greater capacity to produce the ATP required to fuel the Na^+/K^+/ATPase and remove $[Na^+]_i$ from the axons. The converse applies to the smaller axons, which are thought to contribute to the third peak of the CAP. In these axons, the rate of Na^+ influx exceeds the capacity for the axonal Na^+/K^+/ATPase to remove intracellular Na^+ from the axon due to limited ATP supply, constraining the resilience of these axons to high frequency firing (Zang and Marder, 2021).

$[Na^+]_i$ accumulation has been modelled in a computer simulation by Zang and Marder (2021), whose findings were consistent with ours, showing that spike-triggered $[Na^+]_i$ accumulation in modelled myelinated axons decreased with increasing axon diameter. It was proposed that this was due to larger diameter axons being more efficient at propagating high frequency firing as they have larger length constants, in addition to a lower surface area-to-volume ratio. They also predicted that $[Na^+]_i$ accumulated in myelinated axons at a much slowed rate than unmyelinated axons due to the presence of the Nodes of Ranvier. The juxtaparanodal regions of the axoplasm act as a 'reservoir' for axonal Na^+ to diffuse towards. Na^+ can then reside within these myelinated compartments without requiring the immediate action of the Na^+/K^+/ATPase to remove it (Zang and Marder, 2021). The culmination of these factors results in larger diameter myelinated axons being able to retain their ability to sustain high frequency spiking under physiological conditions, as compared to axons whose diameter is smaller, or those which are unmyelinated. However, upon periods of consistent high frequency firing, $[Na^+]_i$ accumulation may still compromise their function, as we saw in figure 20. Although Zang and Marder (2021) provided credible insight into $[Na^+]_i$ accumulation during high frequency firing through computer simulation, our results used an animal model and indirect calculation of $[Na^+]_i$ which accounted for the real-life variables such as astrocytic spatial buffering. Our results in conjunction with those found by Zang and Marder (2021) therefore provide convincing evidence for $[Na^+]_i$ accumulation causing the fall in amplitude

during high frequency firing and that this occurs in a differential manner across the three peaks dependent on axon diameter.

4.4 The role of $[K^+]_o$ in CAP recovery

Although we have shown that $[K^+]_o$ is unlikely to be the cause of CAP failure during high frequency firing, our results from figure 27 suggest that $[K^+]_o$ may alternatively play a role in the post-stimulus recovery of the CAP. We have previously discussed how during a 100 Hz stimulation, the rate of $[K^+]_o$ rise was much faster than the fall in CAP amplitude (figure 27). However, upon the cessation of stimulation, the undershoot of $[K^+]_o$ and overshoot in CAP amplitude appeared to mirror each other (figure 27). This suggests that although $[K^+]_o$ may not be the driving force for the CAP amplitude fall, it may dictate its rate of recovery. It is thought that as the stimulation is terminated, the Na^+/K^+/ATPase pumps work at their maximal rate in an attempt to remove the $[Na^+]_i$ which has accumulated. However, the stoichiometry of the Na^+/K^+/ATPase is that for every 3 molecules of N^+ transported outside of the cell, 2 molecules of K^+ enter against their concentration gradient, per catalytic cycle (Pirahanchi and Aeddula, 2019). Therefore, $[K^+]_o$ is rapidly transported into the axons during $[Na^+]_i$ removal. However, some $[K^+]_o$ has already been buffered by local astrocytes following stimulation, removing it from the extracellular space (Orkand et al., 1966) . Therefore, as the Na^+/K^+/ATPase co-transports $[K^+]_o$ into the axon, it exhibits an undershoot from its baseline extracellular concentration from 3 mM to 2.7 mM (SD=0.25) (figure 23). This was consistent with findings by Ransom et al (2000), who found that following the cessation of a 100Hz stimulus for 1 second, the post-stimulus recovery of accumulated $[K^+]_o$ follows a double exponential time course, with an initial fast time constant (0.9 ± 0.2s) followed by a later slow time constant (4.2 ± 1s). They proposed that this initial fast recovery was of as a result of K^+ uptake by the Na^+/K^+/ATPase expressed on the surface membrane of glial cells. However, the later sustained phase was due to

the Na^+/K^+/ATPase isoform expressed on the axonal membrane, stimulated by $[Na^+]_i$ accumulation in the axons, which cause an undershoot in $[K^+]_o$ from its baseline concentration. This second sustained phase of $[K^+]_o$ clearance by the axonal Na^+/K^+/ATPase acts to hyperpolarise the reversal potential for K^+, which releases the inactivation of some Na^+ channels, priming them to fire upon the next stimulation. This results in an overshoot in the CAP amplitude beyond its original baseline amplitude, which mirrors the $[K^+]_o$ undershoot (figure 27). This effect could be further seen in figure 28, where $[K^+]_o$ was decreased to 2.5 and 2 mM, before the imposition of a 100 Hz stimulus. It can be observed that as $[K^+]_o$ was decreased, the CAP progressively increased in amplitude. During the 100 Hz stimulus, the CAP amplitude decreased as we would expect, however overshot its normalised baseline in amplitude upon the cessation of this stimulus (figure 28). This effect was uniform across all three of the CAP peaks, unlike the effects of increasing $[Na^+]_i$ which affected the three peaks in a differential manner (figure 20). This therefore reinforces the proposition that $[K^+]_o$ dictates this overshoot in CAP amplitude during post-stimulus recovery.

Conclusion

Our results provide strong evidence that activity-dependent $[Na^+]_i$ accumulation is the cause of CAP failure during high frequency firing. Furthermore, we suggest that this accumulation occurs in a differential manner across the three peaks of the CAP, accumulating the least in the axons contributing to the first peak and the most in the least in the smallest diameter axons contributing to the third peak. This is proposed to be a result of axons surface area-to-volume considerations and their subsequent energy supply to facilitate $[Na^+]_i$ removal. These results provide further insight into the mechanisms underlying the fall in CAP during metabolic challenge and propose an alternative explanation to the widely accepted $[K^+]_o$ hypothesis.

Publications and Presentations

Published Papers

Hopper, A.J., Beswick-Jones, H. & Brown, A.M. A color-coded graphical guide to the Hodgkin and Huxley papers. Advances in Physiology Education, 46 (2022) p.580-592

Hopper, A., Beswick-Jones, H. & Brown, A.M.. The Nernst equation: using physico-chemical laws to steer novel experimental design. Advances in Physiology Education, 46 (2022) p. 206-210

Conference Appearances

NC3Rs

8th July 2022 Nottingham

A method for increasing experimental efficiency whilst maintaining statistical power: application to electrophysiological recordings from rodent optic nerve

Amy Hopper, Hana Beswick-Jones & Angus M Brown

Physiology Society

12-13th April 2022 Nottingham

Axon sub-population sensitivity to high frequency stimulus in adult mouse optic nerve

Amy Hopper, Hana Beswick-Jones & Angus M Brown

References

Adams, B., Fitch, T., Chaney, S. and Gerlai, R., 2002. Altered performance characteristics in cognitive tasks: comparison of the albino ICR and CD1 mouse strains. *Behavioural Brain Research*, *133*(2), pp.351-361.

Allen, L., Anderson, S., Wender, R., Meakin, P., Ransom, B.R., Ray, D.E. and Brown, A.M., 2006. Fructose supports energy metabolism of some, but not all, axons in adult mouse optic nerve. *Journal of Neurophysiology*, *95*(3), pp.1917-1925.

Armstrong, C.M., 2005. Channels and pumps early in evolution. In *Pumps, Transporters, and Ion Channels* (pp. 1-10). Springer, Boston, MA.

Bastian, C., Brunet, S. and Baltan, S., 2020. Ex vivo studies of optic nerve axon electrophysiology. In *Axon Degeneration* (pp. 169-177). Humana, New York, NY.

Bay, V. and Butt, A.M., 2012. Relationship between glial potassium regulation and axon excitability: a role for glial Kir4. 1 channels. *Glia*, *60*(4), pp.651-660.

Baylor, D.A. and Nicholls, J.G., 1969. After-effects of nerve impulses on signalling in the central nervous system of the leech. *The Journal of Physiology*, *203*(3), pp.571-589.

Beck, J.F., Donini, J.C. and Maneckjee, A., 1982. The effect of sulfide and cyanide on nerve function. *Toxicology Letters*, *10*(2-3), pp.189-193.

Borrelli, M.J., Carlini, W.G., Dewey, W.C. and Ransom, B.R., 1985. A simple method for making ion-selective microelectrodes suitable for intracellular recording in vertebrate cells. *Journal of Neuroscience Methods*, *15*(2), pp.141-154.

Brown, A.M., 2020. A companion guide to the Hodgkin-Huxley papers. *London, UK: The Physiological Society*.

Brown, A.M., Tekkök, S.B. and Ransom, B.R., 2003. Glycogen regulation and functional role in mouse white matter. *The Journal of Physiology*, *549*(2), pp.501-512.

Connors, B.W., Ransom, B.R., Kunis, D.M. and Gutnick, M.J., 1982. Activity-dependent K+ accumulation in the developing rat optic nerve. *Science*, *216*(4552), pp.1341-1343.

Evans, R.D., Weston, D.A., McLaughlin, M. and Brown, A.M., 2010. A non-linear regression analysis method for quantitative resolution of the stimulus-evoked compound action potential from rodent optic nerve. *Journal of Neuroscience Methods*, *188*(1), pp.174-178.

Frankenhaeuser, B. and Hodgkin, A.L., 1956. The after-effects of impulses in the giant nerve fibres of Loligo. *The Journal of Physiology*, *131*(2), p.341.

Friede, R.L., Benda, M., Dewitz, A. and Stoll, P., 1984. Relations between axon length and axon caliber: Is maximum conduction velocity the factor controlling the evolution of nerve structure?. *Journal of the Neurological Sciences*, *63*(3), pp.369-380.

Gordon, T.R., Kocsis, J.D. and Waxman, S.G., 1990. Electrogenic pump (Na+/K+-ATPase) activity in rat optic nerve. *Neuroscience*, *37*(3), pp.829-837.

Grundy, D., 2015. Principles and standards for reporting animal experiments in The Journal of Physiology and Experimental Physiology. *Experimental physiology*, *100*(7), pp.755-758.

Hartline, D.K. and Colman, D.R., 2007. Rapid conduction and the evolution of giant axons and myelinated fibers. *Current Biology*, *17*(1), pp.R29-R35.

Hodgkin, A., Huxley A (1952a) The components of membrane conductance in the giant axon of Loligo. *The Journal of Physiology*, *116*, p.473.

Hodgkin, A.L. and Huxley, A.F., 1952b. The dual effect of membrane potential on sodium conductance in the giant axon of Loligo. *The Journal of Physiology*, *116*(4), p.497.

Hodgkin, A.L. and Huxley, A.F., 1939. Action potentials recorded from inside a nerve fibre. *Nature*, *144*(3651), pp.710-711.

Hodgkin, A.L. and Huxley, A.F., 1953. Movement of radioactive potassium and membrane current in a giant axon. *The Journal of Physiology*, *121*(2), p.403.

Hodgkin, A.L. and Huxley, A.F., 1947. Potassium leakage from an active nerve fibre. *The Journal of Physiology*, *106*(3), p.341.

Hodgkin, A.L. and Katz, B., 1949. The effect of sodium ions on the electrical activity of the giant axon of the squid. *The Journal of Physiology*, *108*(1), p.37.

Hopper, A., Beswick-Jones, H. and Brown, A.M., 2022. The Nernst equation: using physico-chemical laws to steer novel experimental design. *Advances in Physiology Education*, *46*(1), pp.206-210.

Keynes, R.D., 1951. The leakage of radioactive potassium from stimulated nerve. *The Journal of Physiology*, *113*(1), p.99.

Kofuji, P. and Newman, E., 2004. Potassium buffering in the central nervous system. *Neuroscience*, *129*(4), pp.1043-1054.

Meakin, P.J., Fowler, M.J., Rathbone, A.J., Allen, L.M., Ransom, B.R., Ray, D.E. and Brown, A.M., 2007. Fructose metabolism in the adult mouse optic nerve, a central white matter tract. *Journal of Cerebral Blood Flow & Metabolism*, *27*(1), pp.86-99.

More, H.L. and Donelan, J.M., 2018. Scaling of sensorimotor delays in terrestrial mammals. *Proceedings of the Royal Society B*, *285*(1885), p.20180613.

Mulkidjanian, A.Y., Bychkov, A.Y., Dibrova, D.V., Galperin, M.Y. and Koonin, E.V., 2012. Origin of first cells at terrestrial, anoxic geothermal fields. *Proceedings of the National Academy of Sciences*, *109*(14), pp.E821-E830.

Niklas, K.J. and Newman, S.A., 2013. The origins of multicellular organisms. *Evolution & Development*, *15*(1), pp.41-52.

Orkand, R.K., Nicholls, J.G. and Kuffler, S.W., 1966. Effect of nerve impulses on the membrane potential of glial cells in the central nervous system of amphibia. *Journal of Neurophysiology*, *29*(4), pp.788-806.

Otis, T.S. and Gilly, W.F., 1990. Jet-propelled escape in the squid Loligo opalescens: concerted control by giant and non-giant motor axon pathways. *Proceedings of the National Academy of Sciences*, *87*(8), pp.2911-2915.

Passow, H., 1964. Ion and water permeability of the red blood cell. *The Red Blood Cell*, p.71.

Perge, J.A., Koch, K., Miller, R., Sterling, P. and Balasubramanian, V., 2009. How the optic nerve allocates space, energy capacity, and information. *Journal of Neuroscience*, *29*(24), pp.7917-7928.

Pirahanchi, Y. and Aeddula, N.R., 2019. Physiology, sodium potassium pump (Na+ K+ Pump).

Ransom, C.B., Ransom, B.R. and Sontheimer, H., 2000. Activity-dependent extracellular K+ accumulation in rat optic nerve: the role of glial and axonal Na+ pumps. *The Journal of Physiology*, *522*(3), pp.427-442.

Rich, L.R. and Brown, A.M., 2018. Fibre sub-type specific conduction reveals metabolic function in mouse sciatic nerve. *The Journal of Physiology*, *596*(10), pp.1795-1812.

Rich, L.R., Patrick, J.A., Hamner, M.A., Ransom, B.R. and Brown, A.M., 2020. A method for reducing animal use whilst maintaining statistical power in electrophysiological recordings from rodent nerves. *Heliyon*, *6*(6), p.e04143.

Rosenbluth, J., 2009. Multiple functions of the paranodal junction of myelinated nerve fibers. *Journal of Neuroscience Research*, *87*(15), pp.3250-3258.

Stys, P.K., 2004. White matter injury mechanisms. *Current Molecular Medicine*, *4*(2), pp.113-130.

Stys, P.K., Ransom, B.R. and Waxman, S.G., 1991. Compound action potential of nerve recorded by suction electrode: a theoretical and experimental analysis. *Brain Research*, *546*(1), pp.18-32.

Susuki, K., 2010. Myelin: a specialized membrane for cell communication. *Nature Education*, *3*(9), p.59.

Tekkök, S.B., Brown, A.M. and Ransom, B.R., 2003. Axon function persists during anoxia in mammalian white matter. *Journal of Cerebral Blood Flow & Metabolism*, *23*(11), pp.1340-1347.

Tekkök, S.B., Ye, Z. and Ransom, B.R., 2007. Excitotoxic mechanisms of ischemic injury in myelinated white matter. *Journal of Cerebral Blood Flow & Metabolism*, *27*(9), pp.1540-1552.

Veenith, T. and Menon, D.K., 2011. The cerebral circulation. In *Core Topics in Neuroanaesthesia and Neurointensive Care* (pp. 17-21). Cambridge: Cambridge University Press.

Waxman, S.G. and Bennett, M.V., 1972. Relative conduction velocities of small myelinated and non-myelinated fibres in the central nervous system. *Nature New Biology*, *238*(85), pp.217-219.

Yamate, C.L. and Ransom, B.R., 1985. Effects of altered gliogenesis on activity-dependent K+ accumulation in the developing rat optic nerve. *Developmental Brain Research*, *21*(2), pp.167-173.

Zacchia, M., Abategiovanni, M.L., Stratigis, S. and Capasso, G., 2016. Potassium: from Physiology to Clinical Implications. *Kidney Diseases*, *2*(2), pp.72-79.

Zang, Y. and Marder, E., 2021. Interactions among diameter, myelination, and the Na/K pump affect axonal resilience to high-frequency spiking. *Proceedings of the National Academy of Sciences*, *118*(32), p.e2105795118.

Zhang, L. and McBain, C.J., 1995. Potassium conductances underlying repolarization and after-hyperpolarization in rat CA1 hippocampal interneurones. *The Journal of Physiology*, *488*(3), pp.661-672.